Mushrooms and Brushes in Thin Films of Diblock Copolymer/Homopolymer Mixtures

H. Retsos,[†,‡,§] A. F. Terzis,[∥,⊥] S. H. Anastasiadis,[*,†,‡] D. L. Anastassopoulos,[∥] C. Toprakcioglu,[∥] D. N. Theodorou,[⊥] G. S. Smith,[#] A. Menelle,[⊗] R. E. Gill,[▽] G. Hadziioannou,[▽] and Y. Gallot[○]

Foundation for Research and Technology−Hellas, Institute of Electronic Structure and Laser, P.O. Box 1527, 711 10 Heraklion, Crete, Greece; University of Crete, Physics Department, 710 03 Heraklion, Crete, Greece; University of Patras, Physics Department, 265 00 Rio Patras, Greece; University of Patras, Department of Chemical Engineering and Foundation for Research and Technology−Hellas, Institute of Chemical Engineering and High-Temperature Processes, 265 00 Rio Patras, Greece; Los Alamos National Laboratory, LANSCE, Los Alamos, New Mexico 87545; Laboratoire Leon Brillouin (CEA-CNRS), CEA Saclay, 91191 Gif-sur-Yvette Cedex, France; Groningen University, Chemistry Department, 9747 AG Groningen, The Netherlands; and Institut Charles Sadron (CRM-EAHP), 67083 Strasbourg, France

Received July 6, 2001

ABSTRACT: The configuration of polymer chains end-adsorbed at a surface from the melt is probed by taking advantage of the interfacial segregation of diblock copolymers to the substrate/polymer interface from their mixtures with homopolymers in thin films as a function of the ratio of block lengths. The segment density profiles of either PV2P−PS or PMMA−PS diblocks adsorbed at the PS/substrate interface are evaluated by neutron reflectivity as a function of the relative size of the anchoring block vs that of the dangling block. Moreover, the composition profiles and conformational characteristics of all chain species present in the interfacial region are evaluated using a lattice-based self-consistent field model inspired by the work of Scheutjens and Fleer and extended to incorporate chain conformational stiffness. Inputs to the model are the molecular characteristics of the various species, interaction parameters extracted from experimental binary interfacial widths, and experimental data on the total surface excess. When the ratios of the block-lengths are changed, both experiment and theory reveal evidence for the existence of three regimes regarding the configuration of the dangling chains: a "wet brush" regime, a "mushroom" regime, and a broad transition regime in between.

I. Introduction

A good understanding of the science of polymer surfaces and interfaces can be crucial with respect to the efficient utilization of processes in which surfaces/interfaces are generated and/or modified, or in which they interact with various environmental components. The behavior of polymer chains at surfaces/interfaces is of fundamental importance in scientific areas such as wetting, adhesion, and colloid stabilization, whereas many applications require that a polymeric material be attached-to or placed-in-contact with another material. In certain cases, such as the classic nonstick pan, lubrication, and release paper, it is desirable to create surfaces that do not interact with the material in contact. On the other hand, in applications such as rubber toughening of blends, filled or fiber-reinforced polymers, and coatings, dissimilar materials must adhere to each other for enhanced performance. Likewise, the structure and interactions at polymer/metal (or in general polymer/substrate) interfaces play a crucial role in the shear field affecting the stick-slip behavior during polymer processing, and, therefore, the properties of the processed products.

The properties of surfaces/interfaces can be altered/modified by the addition of interfacially active components, which can selectively segregate to the interface in order to reduce the total free energy of the system. In certain cases, these additives are of the block copolymer type (copolymers consisting of two chemically different chains connected at one of their ends) with one block being miscible with the matrix material and the other being attracted to the surface/interface. Such interfacial partitioning produces chain configurations in which the miscible block forms a dangling tail usually referred to as a polymer brush or a mushroom.[1−3] A great number of investigations have appeared on the segregation of block copolymers to a surface/interface with most of the attention being paid to the adsorption of block copolymers from solution (see, e.g., refs 1−11). It is noted that the cases of homopolymer physisorption or of end-anchored homopolymers in solution are not discussed in this manuscript; the interested reader should refer to the relevant literature (e.g., refs 1−3). Fewer investigations, however, have appeared on surface-anchored layers in the melt, which can be formed by the segregation of either a block copolymer from homopolymer/copolymer mixtures to a free surface[12−14] and/or to an interface with a solid substrate[12,14−19] or with another immiscible polymer,[20,21] or of an end-function-

* To whom correspondence should be addressed.
† Foundation for Research and Technology−Hellas.
‡ University of Crete.
§ Present Address: Department of Materials, University of California at Santa Barbara, Santa Barbara, CA 93106.
∥ University of Patras, Physics Department.
⊥ Institute of Chemical Engineering and High-Temperature Processes, and University of Patras, Department of Chemical Engineering.
Los Alamos National Laboratory.
⊗ Laboratoire Leon Brillouin.
▽ Groningen University.
○ Institut Charles Sadron.

10.1021/ma011174j CCC: $22.00
Published on Web 12/21/2001

alized homopolymer from a polymer mixture.[22−24] It has been anticipated that although the configuration of grafted chains in the melt may, in principle, be similar to that in solution, the polymeric nature of the matrix ("solvent") molecules should influence their behavior.[25−29]

When an AB diblock copolymer is mixed with a B homopolymer, interfacial partitioning of the copolymer may occur to the polymer/air and/or the polymer/substrate interface when the A block of the copolymer possesses a lower surface tension and/or is attracted more strongly to the substrate interface, respectively. In this case, the interfacially active A block acts as an anchor to the free surface and/or to the substrate, whereas the B block (compatible with the homopolymer) forms a dangling chain within the matrix.[12−19] The conformation of the dangling block depends on the grafting density σ and on the relative size of the dangling block to that of the matrix homopolymer.[25−29] In the case of block copolymers, σ can be influenced by the size of the anchoring block. For diblock copolymers adsorbed onto a solid surface from solution, the mushroom or brush configuration of the dangling chains has indeed been shown to be influenced[5,10] by the block-length ratio with a maximum in the adsorbed amount expected for a certain value of this ratio. The present work addresses the conformation of the dangling chains of the nonadsorbing block for diblock copolymers segregating to the interface from a mixture with a homopolymer, where the surface density of chains is varied by utilizing diblocks with varying block-length ratio. Important differences are anticipated between the present study and the respective one in solution,[10] since the interactions of the copolymer blocks with the matrix (a homopolymer vs a selective solvent) are, in principle, different and the matrix is now polymeric.

Theory has addressed the case of end-anchored chains in the melt[25−29] (when the anchoring is achieved by an irreversible attachment of an end segment). The variables that determine the configuration of the dangling chains are the grafting density, σ, the number of segments of the dangling chain, N, and the number of segments of the matrix, P. Two classical limiting regimes were originally[25] discussed: for low σ, the dangling-chains do not overlap and their conformation is not disturbed relative to that in the bulk ("mushroom" regime), whereas, for high σ, the anchored chains are stretched ("brush" regime); "wet" and "dry" brushes were proposed,[25,26] depending on the penetration of the matrix polymer. More detailed calculations identified[29] various sub-regimes in the σ vs P plane with N as a parameter. For $P > N$ (which is of interest in the context of the present manuscript), three regimes have been proposed: nonoverlapping (ideal) mushrooms for $\sigma a^2 < N^{-1}$ (a is the segment length), where the conformation of the dangling chain is ideal; dry brushes for $\sigma a^2 > N^{-1/2}$, where the N chains are stretched and the P chains are almost completely expelled from the brush; and partially overlapping mushrooms for $N^{-1} < \sigma a^2 < N^{-1/2}$where the chains overlap but without any significant stretching (also called nonstretched brush). For $P < N$, the σ vs P plane is much more complicated and is not discussed further herein.

For the adsorption of block copolymers, the grafting density σ should be influenced by the size N_A of the anchoring block (for the dangling chain, $N \equiv N_B$) and, therefore, various regimes may be spanned as N_A is changed. The dependence of σ on N_A and N_B in the melt was qualitatively discussed by Kunz et al.[14] for polystyrene-*block*-polyisoprene diblock copolymers segregating to the free surface from mixtures with homopolymer polystyrene. For large fractions of the anchoring block A, the ideal mushroom regime was envisioned with the anchoring block forming thin "pancakes" on the surface with diameter $\sigma^{-1/2}$ and small, more or less constant, thickness on the order of a few segments; in that case, $\sigma a^2 \propto N_A^{-1}$ (this dependence of σ on N_A was experimentally verified in solution[10]). Note that the assumption of a pancake configuration of the anchored chain (with thickness independent of N_A) is usually made.[5,6] The thickness of the dangling chain is $L \cong aN_B^{1/2}$, whereas the average volume fraction of the tethered chains inside the adsorbed layer should scale as $\bar{\phi} \cong N_B^{1/2}\sigma a^2 \propto N_B^{1/2}N_A^{-1}$ and $\bar{\phi} < N_B^{-1/2} < < 1$. In the melt, this regime can be achieved for grafting densities $\sigma a^2 < N_B^{-1}$, i.e., for volume fractions $f_B < 0.5$. At the other limit of small fractions of the anchoring block (large f_B), i.e., in the limit of high grafting densities ($\sigma a^2 > N_B^{-1/2}$ for $P > N_B$), one may approach the dry brush regime (with overlapping stretched dangling chains and completely expelled matrix chains) with brush thickness $L \approx a^3N_B\sigma$. The equilibrium grafting density can be estimated from the balance of the main contributions to the free energy of the anchored copolymer chains on the surface, i.e., of the gain in energy due to the adsorption of the anchor segments to the surface,[12] $F_{sticking}/kT \cong (\chi N_A + rN_A\delta)$, and of the repulsive elastic energy, $F_{elastic}/kT \cong N_B(\sigma a^2)^2$, of the dangling chains (the mixing energy with the matrix chains is negligible). Thus,[14] $\sigma a^2 \approx [\epsilon N_A/N_B]^{1/2}$, where $\epsilon = \chi + r\delta$ (χ is the A−B interaction parameter, r is the fraction of A monomers sticking to the surface, and δ the difference in surface energies of A and B per monomer). Moreover, $\bar{\phi} \cong O(1)$. For intermediate σ's in the overlapping mushrooms regime (also called nonstretched brush[29]), the tethered chains overlap, but there is no significant stretching and no penalty due to mixing with similar chains (for $P > N_B$, this regime is attained for $N_B^{-1} < \sigma a^2 < N_B^{-1/2}$). Thus, the tethered chains behave as if they were isolated ($L \cong aN_B^{1/2}$), and from a free energy point of view, there is no real border between this regime and the nonoverlapping mushroom regime.[30] Subsequently, the scaling of σ with the block molecular weights should be more or less similar with that for nonoverlapping mushrooms whereas $N_B^{-1/2} < \bar{\phi} < 1$; i.e., $\bar{\phi}$ is larger than for ideal mushrooms. Within the above arguments, a maximum in the copolymer surface excess was anticipated for a series of diblocks with almost constant $N_{BCP} = N_A + N_B$ but different compositions f_B with the characteristics (height and position) of the maximum depending on the sticking energy parameter ϵ (or equivalently the surface affinity), on N_{BCP}, and on P. The lack of experimental observation of such a maximum in the melt (in contrast to the case in from solution[5,10]) was attributed to the maximum being very shallow or outside the range of the experimental parameters.[14]

An alternative analysis[30] for the brush regime writes the interfacial term as $F_{interf}/kT \cong \sigma^{-1}(\gamma_{A,B} + \gamma_{A,sub})/(kT)$ and includes the elastic energy of the brush, $F_{elastic}/kT \cong N_B(\sigma a^2)^2$, and the cost of confining[30] the anchor layer, $F_{confine}/kT \cong \ln h^2/h \approx 2\ln(N_A\sigma a^2)/(N_A\sigma a^2)$, where $\gamma_{A,B}$ and $\gamma_{A,sub}$ are the interfacial energies between A and B and between A and substrate, respectively, and $h \approx N_A\sigma a^2$ is the thickness of the anchor layer. Minimizing the total free energy with respect to σ results in $\sigma a^2 \cong ([a^2(\gamma_{A,B}$

Table 1. Molecular Characteristics of the Polystyrene/Poly(deuterated styrene)-*b*-poly(2-vinylpyridine) Samples

code	M_W	M_W/M_n	w_{PS}[a]	N_{total}[b]	f_{PS}[c]	N_{PV2P}[b]	N_{PS}[b]	P
SV2P-3.4	78 400	1.05	0.957	782	0.960	32	750	
SV2P-18	93 000	1.05	0.806	915	0.820	165	750	
SV2P-32	107 000	1.05	0.701	1043	0.719	293	750	
SV2P-45	120 000	1.05	0.625	1163	0.645	413	750	
SV2P-68	143 000	1.05	0.524	1373	0.546	623	750	
SV2P-95[d]	170 000	1.05	0.441	1621	0.463	871	750	
SV2P-102[d]	177 000	1.05	0.424	1685	0.445	935	750	
PSH	186 000	1.04	1.000	1815	1.000			1815

[a] Polystyrene weight fraction. [b] Based on average segmental volume. [c] Polystyrene volume fraction. [d] Diblocks used in ref 17.

$+ \gamma_{A,sub})/(kT) + 2\ln N_A/N_A]/[2N_B])^{1/3}$, i.e., a weak dependence on N_A. In the mushroom regime, $\sigma a^2 \cong ([a^2(\gamma_{A,B} + \gamma_{A,sub})/(kT)]/[2N_A])^{1/3}$ is expected, whereas $\sigma a^2 \cong ([a^2(\gamma_{A,B} + \gamma_{A,sub})/(kT)]/[2(N_A + N_B)])^{1/3}$ in the regime in between. Thus, this prediction is that σ will be almost constant for low N_A ($\sigma a^2 > N_B^{-1/2}$) whereas it will decrease with increasing N_A for higher values of N_A.

One can expect that a more or less direct probe of the brush or mushroom configuration of the dangling chains will be the investigation of the segment density profiles of the adsorbed diblock copolymer chains. It is anticipated that the dangling-chain configuration will influence the shape of the segment density profiles. The dependencies of the profile characteristics on the surface density σ and on the dangling chain molecular weight N_B for diblock copolymers adsorbed to a surface from solution have been investigated earlier experimentally[11] and confirmed theoretically[6] using a numerical self-consistent mean-field calculation. The surface density was experimentally controlled (independently of N_A and N_B) by compressing a Langmuir monolayer at the air/liquid interface, whereas most of the data (and the calculation) were concerned with the brush regime. Various functional forms for the volume fraction profile of the dangling chains were tested in the analysis of the neutron reflectivity data. It was evident that a depletion layer next to the wall was present, where the profile rises sharply, whereas the profile smoothly extended toward the bulk solution as a parabola with an exponential tail; this resulted in a maximum ϕ_{max} in the profile at a position z_{max} away from the surface. For $\sigma^* = \pi R_g^2 \sigma \geq 2$ (R_g is the radius of gyration of the dangling block free in solution), the experimental data for the root-mean-squared layer thickness ($z_{rms} \propto N_B^{0.86}\sigma^{0.22}$) agreed with the calculation ($z_{rms} \propto N_B^{0.81}\sigma^{0.24}$). For $\sigma^* \geq 2$, the calculation resulted in a maximum volume fraction of $\phi_{max} \propto N_B^{0.10}\sigma^{0.68}$ and a position of the maximum $z_{max} \propto N_B^{0.43}\sigma^{-0.04}$. It is noted that the molecular weight of the anchor block was irrelevant in that study since the anchoring density was independently adjusted,[11] whereas in the calculation[6] the anchoring block was assumed to lie flat on the surface (pancake) with a small thickness on the order of the segment length a.

In the present work, the detailed segment density profiles of the adsorbed diblock copolymer chains are investigated in the melt using neutron reflectivity and taking advantage of the interfacial segregation of diblock copolymers to the substrate/polymer interface from their mixtures with the respective homopolymers in thin films. The adsorbed chain configuration is probed as a function of the ratio of block lengths utilizing two series of diblocks: (i) a series of poly(2-vinylpyridine)-*block*-poly(deuterated styrene), with the same molecular weight of the dangling polystyrene chain (N_B) and different molecular weights of the anchoring block (N_A), in hydrogenous polystyrene matrix and (ii) a series of poly(methyl methacrylate)-*block*-polystyrene, with constant total molecular weight $N_{BCP} = N_A + N_B$ and different compositions f_B, in poly(deuterated styrene). Moreover, the composition profiles and conformational characteristics of all chain species present in the interfacial region are investigated using a lattice-based self-consistent field model inspired by the work of Scheutjens and Fleer[31,32] as extended to incorporate chain conformational stiffness.[33,34] Inputs to the model are the relative amounts, molecular weights, conformational stiffnesses and bulk densities of all polymer species, interaction parameters extracted from experimental binary interfacial widths, as well as experimental data on the total surface excess.

The shapes of the segment density profiles of the dangling blocks are significantly influences by the block length ratio and this is much more evident in series (i). The profiles of the dangling chains exhibit a maximum vs the distance from the wall. The characteristics of the profiles provide evidence for the existence of three regimes: a brushlike regime for short anchor blocks with a high value (~55%) of the maximum of the profile in the proximity to the wall; a mushroomlike regime for large anchor molecular weights with a low value (~28%) of the maximum at a certain (larger) distance away from the wall; a broad transition regime in between. These correlate well with changes in the surface density of chains from high to low values. Experiment and theory agree quite well in these findings. Moreover, an intriguing finding of the theoretical calculation is regarding the shape of the anchoring block, which, contrary to the usual assumption of a pancakelike conformation, resembles more a physically adsorbed homopolymer with a molecular-weight dependent thickness.

The remaining of this article is arranged as follows: Following the Experimental Section, section II, the results of the neutron reflectivity investigations are presented in section III. The theory is presented in section IV and its results are illustrated and discussed in relation to the experimental data in section V. Concluding remarks are presented in section VI.

II. Experimental Section

Materials. A series of poly(2-vinylpyridine)-*block*-poly(deuterated styrene), SV2P, diblock copolymers were synthesized by anionic polymerization under inert atmosphere in tetrahydrofuran (THF) at −70 °C, with monomers added sequentially[17] (the styrene monomers were perdeuterated). Their molecular characteristics are shown in Table 1.

A series of poly(methyl methacrylate)-*block*-polystyrene, SM, diblock copolymers were prepared by living anionic polymerization under inert atmosphere.[35] The polystyrene blocks were polymerized first in THF at low temperature (−70 °C) using (phenylisopropyl)potassium as initiator. To avoid attack of the ester group of methyl methacrylate (MMA) by the polystyrene

Table 2. Molecular Characteristics of the Poly(deuterated styrene)/Polystyrene-*b*-Poly(methyl methacrylate) Samples[35]

code	M_W	M_W/M_n	w_{PS}[a]	N_{total}[b]	f_{PS}[c]	N_{PMMA}[b]	N_{PS}[b]	P
SM-67	172 000	1.05	0.669	1714	0.69	531	1183	
SM-51	171 000	1.05	0.512	1680	0.53	790	890	
SM-33	175 000	1.05	0.326	1690	0.35	1098	592	
PSD	190 000	1.03	1.000	2125	1.000			2125

[a] Polystyrene weight fraction. [b] Based on average segmental volume. [c] Polystyrene volume fraction.

carbanions, 1,1-diphenylethylene was introduced prior to the addition of MMA to decrease the nucleophilicity of the active cites. The polymerizations were conducted under high-purity argon in glass vessels equipped with Teflon valves. The characteristics of the diblocks measured by volume exclusion chromatography coupled with light scattering and viscometry are shown in Table 2.

Hydrogenous and perdeuterated polystyrene homopolymers were purchased from the Polymer Standards Service and were used in this study as received. Their characteristics are also shown in Tables 1 and 2, respectively.

Thin films of homopolymer/copolymer mixtures (4 wt % SV2P copolymer in PSH and 2.5 wt % SM in PSD) were prepared by spin coating from toluene solutions onto polished and cleaned Si wafers (10 or 5 cm in diameter, respectively, and 5 mm thickness, purchased from Semiconductor Processing Technologies), placed at 60 °C under vacuum to remove the remaining solvent, annealed for 24 h at 170 °C to reach equilibrium, and then rapidly quenched to room temperature; the NR measurements were performed at room temperature. In the series of experiments discussed in this manuscript, low copolymer concentrations were used in order to limit the formation of micelles (at least for the diblocks with the short immiscible block).

Neutron Reflectivity. The neutron reflectivity (NR) experiments were performed at the time-of-flight SPEAR reflectometer[9−11] at Los Alamos (for the SV2P/PSH films) and at the time-of-flight DESIR reflectometer at the ORPHEE reactor at Saclay[11,36] (for the SM/PSD films).

In brief, a collimated ($\delta\theta$ ca. 0.01° at Los Alamos and 0.01−0.03° at Saclay) neutron beam with a certain distribution of wavelengths ($2 < \lambda < 32$ Å at Los Alamos and $4 < \lambda < 35$ Å at Saclay) impinges upon the specimen surface at a fixed angle θ (1.5° at Los Alamos and 1.8° at Saclay) and the reflected intensity is measured also at an angle θ with respect to the film surface. The variation of the component of the incident neutron momentum perpendicular to the film surface, $k_0 = (2\pi/\lambda)(\sin\theta)$, is achieved due to the wavelength distribution of the incoming neutron beam. Reflectivities, R, as low as 10^{-5}−10^{-6} are measured in both facilities. The principles of NR have been discussed previously[37,38] and are not reproduced here, whereas the analysis of the neutron reflectivity data is performed using the matrix method.[37,38] It is only noted that the instrumental resolution in k_0 space is $\delta k_0/k_0 \approx \delta\theta/\theta + \delta\lambda/\lambda$; the resolution function at each θ, assumed Gaussian with a full-width at half-maximum of δk_0, is convoluted with the calculated reflectivity profiles and then compared to the experimental reflectivity curves. $\delta\lambda$ is set at 0.01 Å, and thus, $\delta k_0/k_0$ is about 0.02.

III. Neutron Reflectivity Results

Figure 1 shows the neutron reflectivity data for a ca. 1600 Å film of SV2P-3.4/PSH as reflectivity R vs k_0. The k_0 range (at $\theta = 1.5°$) extends below the critical angle allowing normalization of R to 1 for small k_0's. Five to six orders of reflectivity can be measured with most prominent feature the high-frequency oscillations corresponding to the total film thickness. The data, however, cannot be fitted with a simple homogeneous film but can only be analyzed using a profile, which exhibits a layer enriched in deuterium near the substrate interface; thus, interfacial partitioning of the diblock copolymer is evident at the polymer/silicon interface.

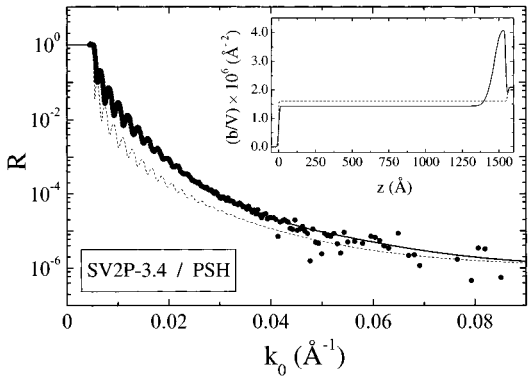

Figure 1. Experimental neutron reflectivity data (●) as a function of k_0 for a ca. 1600 Å thick film of SV2P-3.4/PSH. The solid line is the calculated reflectivity curve, convoluted with the appropriate resolution function, using the scattering length density profile shown in the inset ($z = 0$ denotes the air/polymer surface). The thin dashed line is the respective reflectivity curve using a uniform (average) scattering length density profile (dashed line in the inset).

Poly(2-vinylpyridine), which has been known to be attracted to the silicon wafer surface,[10,17,36,39] forms the anchor whereas dangling deuterated-polystyrene chains extend toward the matrix homopolymer.

The solid line in Figure 1 is the calculated reflectivity curve, convoluted with the appropriate resolution function, using the scattering length density profile in the inset ($z = 0$ denotes the air/polymer surface), whereas the thin dashed line is the respective calculated reflectivity curve using a uniform scattering length density profile equal to the average of the film (dashed line in the inset). It is evident that the data cannot be analyzed with the uniform profile, and an enrichment layer is necessary. As has been extensively discussed by Kent et al.,[11] various functional forms can be used in order to fit these types of reflectivity profiles without significant changes in the precision of the fit. In the present work, a skewed Gaussian model has been used, which allows for the presence of an asymmetric maximum in the scattering length density profile with a relatively sharp depletion layer next to the silicon surface and a more extended profile toward the matrix. A thin region of scattering length approaching that of the pyridine block is also evident near the silicon surface. The characteristic features of the profile near the silicon/polymer interface will be discussed in relation to Figure 3, below; these features are not significantly influenced by the exact functional form of the profile used in the analysis. It should be noted that, when analyzing the reflectivity data, one should make sure that the extracted profile is consistent with the total deuterium present in the system; this is accomplished by ensuring the equality

$$\int_{\text{film}} (b/V)\, dz = \phi_c^0 f_{PS}(b/V)_{PS,c} + \phi_c^0(1 - f_{PS})(b/V)_{\text{anchor}} + (1 - \phi_c^0)(b/V)_{PS,h} \quad (1)$$

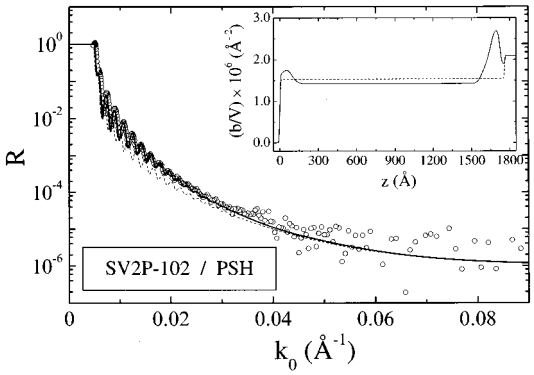

Figure 2. Experimental neutron reflectivity data (○) as a function of k_0 for a ca. 1800 Å thick film of SV2P-102/PSH. The solid line is the calculated reflectivity curve, convoluted with the appropriate resolution function, using the scattering length density profile shown in the inset ($z = 0$ denotes the air/polymer surface). The thin dashed line is the respective reflectivity curve using a uniform (average) scattering length density profile (dashed line in the inset).

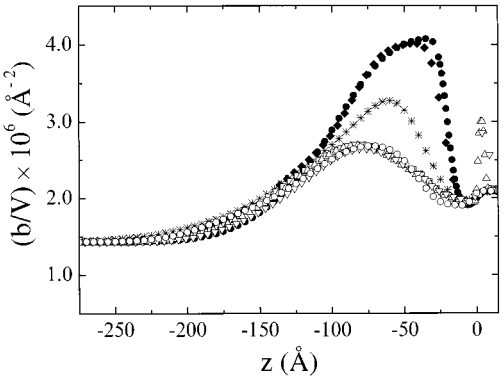

Figure 3. Scattering length density profiles at the silicon/polymer interface extracted from the analysis of the neutron reflectivity data for all SV2P/PSH systems: (●) SV2P-3.4; (♦) SV2P-18; (∗) SV2P-32; (□) SV2P-45; (△) SV2P-68; (▽) SV2P-95; (○) SV2P-102. The data have been shifted along the z axis so that $z = 0$ denotes the polymer/substrate interface.

ϕ_c^0 is the volume fraction of the added copolymer, f_{PS} is its composition in styrene, and $(b/V)_{PS,c} \equiv (b/V)_{PSD} = 6.1 \times 10^{-6}$ Å^{-2}, $(b/V)_{anchor} \equiv (b/V)_{PV2P} = 1.9 \times 10^{-6}$ Å^{-2}, and $(b/V)_{PS,h} \equiv (b/V)_{PSH} = 1.43 \times 10^{-6}$ Å^{-2} are the scattering length densities of the dangling styrene block (deuterated styrene), of the anchor block (vinylpyridine), and of the homopolymer (hydrogenous styrene), respectively. The integral is taken over the whole thickness of the film.

Figure 2 shows the neutron reflectivity data for a ca. 1800 Å film of SV2P-102/PSH as reflectivity R vs k_0, where the solid line is the calculated reflectivity curve, convoluted with the appropriate resolution function, using the scattering length density profile in the inset; the equality condition of eq 1 is fulfilled. Also shown in Figure 2 is the calculated reflectivity curve (thin dashed line) assuming the uniform average scattering length density profile shown in the inset (thin dashed line); the differences in this case are less pronounced than those in Figure 1 signifying right away lower enrichment. Two differences from the profile of SV2P-3.4/PSH (inset of Figure 1) should be discussed. First, the reflectivity data could only be fitted if an enrichment layer was allowed both at the silicon and at the air/polymer interface. The second difference relates to the shape of the enrichment layer at the silicon/polymer interface: although the scale for the z axis in the inset is not appropriate, it will become evident below (in Figure 3) that the region of scattering length similar to that of the pyridine block is now thicker whereas the features of the profile are less pronounced and shifted toward the interior of the film.

The presence of a deuterium-enriched layer at the free surface (besides that at the silicon interface) was observed for the four diblocks with the longest pyridine blocks of Table 1. A direct-space technique could unequivocally prove the existence of such an enrichment layer. However, in the context of this work one can rely on the inability to analyze the reflectivity data without one along with earlier similar findings in the literature in order to accept this finding. Indeed, such a situation has been observed in SV2P/PSH copolymer/homopolymer films by nuclear reaction analysis[39] for higher concentrations (15%) of a lower molecular weight SV2P diblock (SV2P-391_68, $N_{PV2P} = 68$, $N_{PS} = 391$, $P = 4640$), whereas for lower concentrations (5%) segregation was observed only at the silicon interface. Moreover, transmission electron microscopy (TEM) on thin films of mixtures of two of the diblocks of the present investigation (2% of SV2P-95 and 15 and 30% of SV2P-102) with polystyrene (of similar molecular weight) has unequivocally revealed[17] micelles (with pyridine core and deuterated styrene corona) segregated to the free surface. Similar segregation of micelles to the free surface was also observed for a SV2P-391_68/PSH mixture between the air surface and an interface with poly(2-vinylpyridine) homopolymer.[40] In all cases, the understanding was that the micelles are attracted to the free surface due to the (slightly) lower surface energy of deuterated polystyrene vs the hydrogenous one, whereas a theoretical approach developed by Semenov[41] concluded that the micellar contribution to the surface excess is due to a higher rate of formation of micelles at the surface. Note that in all cases the presence of micelles at the surface was observed above a certain concentration estimated to be the critical micelle concentration, which is a function of the molecular weights of the interacting species; this is the reason that the surface enrichment layer was only observed for the diblocks with high pyridine molecular weights. The enrichment layer at the air surface will not be further discussed in the present manuscript.

Figure 3 shows the scattering length density profiles at the silicon/polymer interface extracted from the analysis of the neutron reflectivity data for all SV2P copolymers. It is emphasized that all diblocks have the same molecular weight of the dangling deuterated-polystyrene chains, whereas the molecular weight of the anchor block varies by a factor of 30 (3,400 to 102,000). The profiles have been shifted along the z axis so that the zero for the polymer/silicon interface is placed at the position, where there is the first indication for the substrate (or the very thin silicon oxide layer—observed for SV2P-68 and SV2P-95). Several comments are in order. As the molecular weight of the anchor block increases, the pyridine-like layer at the silicon interface becomes broader, which right away indicates that the configuration of the anchor block is more extended than a simple "pancake" at the surface. Second, the shape of the profiles differs significantly between the two diblocks with the smallest pyridine blocks on one hand and the four diblocks with the largest pyridine blocks on the other, with SV2P-32 falling in between. For SV2P-3.4

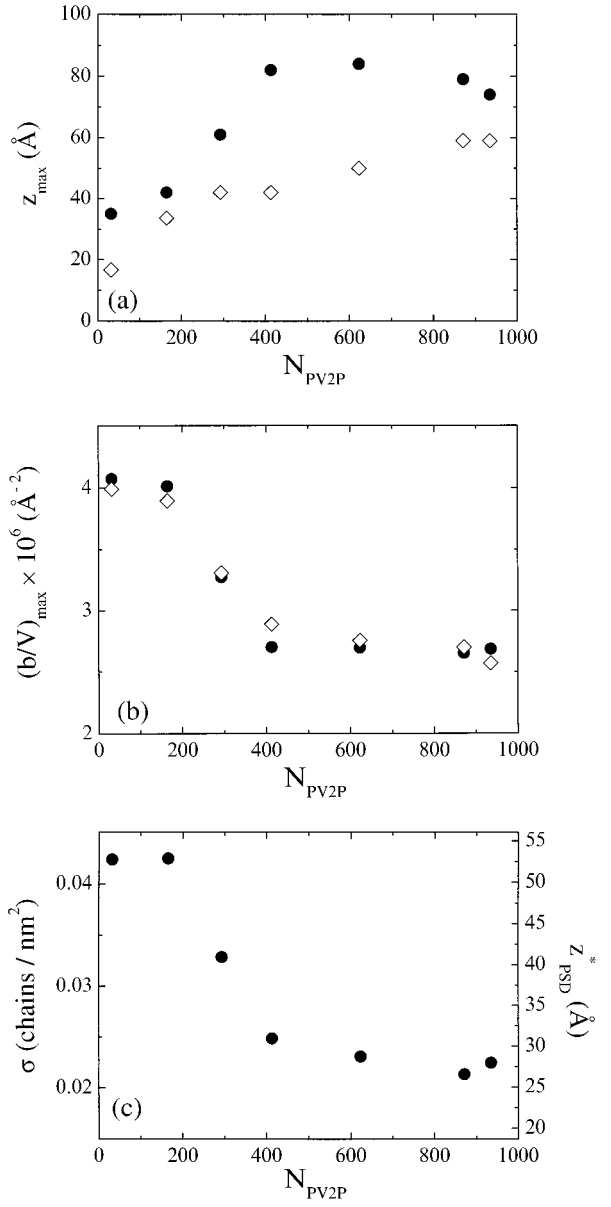

Figure 4. Dependence on the molecular weight of the anchor pyridine block, N_{PV2P}, of (a) the position of the maximum of the scattering length density profiles, z_{max}, as distance from the interface, (b) the value of the scattering length density at the maximum $(b/V)_{max}$, and (c) the surface excess of the dangling block z_{PSD}^* or, equivalently, the surface density of copolymer chains σ. Filled symbols are the experimental data and open symbols the theoretical calculations.

and SV2P-18, the profile exhibits a sharp depletion layer next to the silicon surface and a more extended profile toward the matrix (as discussed in relation to Figure 1), whereas the scattering length density at the maximum indicates about 55% deuterated styrene. For SV2P-45 up to SV2P-102, the profiles are more symmetric, i.e., the maximum is shifted away from the surface to about 80 Å, which does not depend much on the pyridine molecular weight; the scattering length density at the maximum is much smaller, indicating only about 28% deuterated styrene. As noted before, the profile for SV2P-32 falls in between.

Figure 4 shows the dependence on the molecular weight of the anchor pyridine block, N_{PV2P}, of (a) the position of the maximum of the scattering length density profiles, z_{max} (measured as distance away from the silicon or silicon oxide surface), (b) the value of the scattering length density at the maximum $(b/V)_{max}$ and (c) the surface excess of the dangling block $z_{PSD}^* = z_{PS,c}^* \equiv \int_{interface} \phi_{PS,c}(z)\, dz$ and the surface density of copolymer chains σ. The excess of the dangling chains is related to the total surface excess z^* by

$$z_{PSD}^* = z_{PS,c}^* = z^* f_{PS} \tag{2}$$

where z^* is given by

$$z^* \equiv \int_{interface} [\phi_c(z) - \phi_{c,bulk}]\, dz = \int_{interface} [\phi_{PS,c}(z) + \phi_{anchor}(z) - \phi_{c,bulk}]\, dz \tag{3}$$

$\phi_c(z)$ is the total copolymer volume fraction profile in the interfacial region, $\phi_{c,bulk}$ is the copolymer concentration away from the interface, and $\phi_{PS,c}(z) \equiv \phi_{PSD}(z)$ and $\phi_{anchor}(z) \equiv \phi_{PV2P}(z)$ are the volume fraction profiles of the dangling chain (deuterated styrene) and the anchoring block (pyridine), respectively. z^* can be estimated from the experimentally obtained integral

$$\tilde{z} \equiv \int_{interface} [(b/V) - (b/V)_{bulk}]\, dz \tag{4}$$

where (b/V) is the experimental scattering length profile at position z and $(b/V)_{bulk} \cong (b/V)_{PS,h}$ that away from the interface. The (b/V) profile is related to the volume fraction profiles of the various components by

$$(b/V) = \phi_{PS,c}(z)(b/V)_{PS,c} + \phi_{anchor}(z)(b/V)_{anchor} + \phi_{PS,h}(z)(b/V)_{PS,h} \tag{5}$$

with $\phi_{PS,h}(z)$ the volume fraction profiles of the matrix homopolymer (hydrogenous-styrene), whereas the three volume fractions are related by

$$\phi_{PS,c}(z) + \phi_{anchor}(z) + \phi_{PS,h}(z) = 1 \tag{6}$$

Combining eqs 3−7, one gets

$$z^* = \{[(b/V)_{PS,c} - (b/V)_{PS,h}]f_{PS} + [(b/V)_{anchor} - (b/V)_{PS,h}](1 - f_{PS})\}^{-1}\tilde{z} \tag{7}$$

where use has been made of the fact that the deuterated styrene and the pyridine are the two blocks of the diblock and, thus, their total amounts are related by

$$\frac{z_{PS,c}^*}{z_{anchor}^*} = \frac{\int_{interface} \phi_{PS,c}(z)\, dz}{\int_{interface} \phi_{anchor}(z)\, dz} = \frac{f_{PS}}{1 - f_{PS}} \tag{8}$$

where $z_{PV2P}^* = z_{anchor}^* \equiv \int_{interface} \phi_{anchor}(z)\, dz$. Therefore, $z_{PSD}^* = z_{PS,c}^*$ in Figure 4 is estimated using eqs 2 and 7 with $\tilde{z}$ from eq 4. The surface density of the copolymer chains is obtained from the values of $z_{PSD}^* = z_{PS,c}^*$ by

$$\sigma = \frac{z_{PS,c}^*}{N_{PS}\bar{v}} = \frac{z_{anchor}^*}{N_{anchor}\bar{v}} = \frac{z^*}{N_{total}\bar{v}} \tag{9}$$

where N_{PS} and $N_{anchor} = N_{PV2P}$ are the number of segments of the two blocks, N_{total} is that of the whole copolymer, and $\bar{v}$ is the average segmental volume. σ is also shown in Figure 4c vs the number of segments of the anchoring block N_{PV2P}.

All the quantities in Figure 4 show a characteristic change in their behavior between low N_{PV2P} and high N_{PV2P}. The position z_{max} of the maximum of the (b/V) profile moves away from the surface when N_{PV2P} increases for low values of N_{PV2P}, whereas it is almost insensitive to N_{PV2P} for higher values. It is noted that possible uncertainties in the value of z_{max} originate mainly from the positioning of the zero of the z axis in Figure 3. The uncertainties in z_{max} associated with the analysis of the neutron reflectivity data for all samples are less than 6 Å. Similarly to z_{max}, both the maximum scattering length density, $(b/V)_{max}$, and the surface excess of the dangling block, z_{PSD}*, (or equivalently the surface density of copolymer chains, σ) show a "transition" from high values at low N_{PV2P} toward low values for high N_{PV2P}. As was evident in Figure 3 (and will be discussed in the theoretical results section below), when the molecular weight of the anchor increases, the profile of the pyridine block extends more toward the matrix, thus pushing the profile of the deuterated polystyrene block away from the interface. However, if the movement of the position of the maximum were only due to this widening of the profile of the anchor, then z_{max} would continuously increase and would not show the behavior of Figure 4a. Therefore, the change in the behavior of z_{max} (Figure 4a) as well as of $(b/V)_{max}$ (Figure 4b) and z_{PSD}* or σ (Figure 4c) should be related to a different configuration of the dangling block for low and high values of N_{PV2P} as a result of the changes in the surface density σ (Figure 4c). Note that the behavior of σ resembles that estimated by Aubouy[30] and discussed in the Introduction. Therefore, the data indicate a smooth transition from a "brush"-like configuration at low values of N_{PV2P} (high σ) toward a "mushroom"-like configuration at high values of N_{PV2P} (low σ). It is noted that the values of z_{PSD}* and σ are in the range of values usually obtained for equilibrium brushes either in the melt,[12,14,22,23] or in solution.[9] Moreover, from these σ values one can calculate the total copolymer adsorbance, $\Gamma \approx 5-6$ mg/m^2, corresponding to an adsorbance of the dangling block, $\Gamma_{PS,c} \approx 2.5-4.8$ mg/m^2, which fall in the range of earlier investigations.[9]

Figure 5a shows the neutron reflectivity data for a ca. 850 Å thick film of SM-67/PSD as reflectivity R vs k_0. The k_0 range (at $\theta = 0.5°$) extends below the critical angle, allowing normalization of R to one for small k_0's. The solid line in Figure 5a is the calculated reflectivity curve, convoluted with the appropriate resolution function, using the scattering length density profile shown in the inset, which exhibits an enrichment layer at the silicon/polymer interface. Note that the profile looks different from the ones in Figures 1−3 because of the different deuteration scheme. In this case, both blocks of the copolymer are hydrogenous and the contrast is enhanced by using a homopolymer that is deuterated; i.e., $(b/V)_{PS,c} \equiv (b/V)_{PSH} = 1.43 \times 10^{-6}$ Å^{-2}, $(b/V)_{anchor} \equiv (b/V)_{PMMA} = 1.0 \times 10^{-6}$Å^{-2}, and $(b/V)_{PS,h} \equiv (b/V)_{PSD} = 6.1 \times 10^{-6}$Å^{-2}. It is noted that analysis of such types of profile is less unambiguous than of the types of Figures 1−3; ensuring that the extracted profile is consistent with the total deuterium in the system by using eq 1 is even more critical.

Figure 5b shows the scattering length density profiles near the silicon interface extracted from the analysis of the neutron reflectivity data for all SM/PSD films. It is emphasized that, in this case, the diblocks have almost the same total molecular weight, whereas their

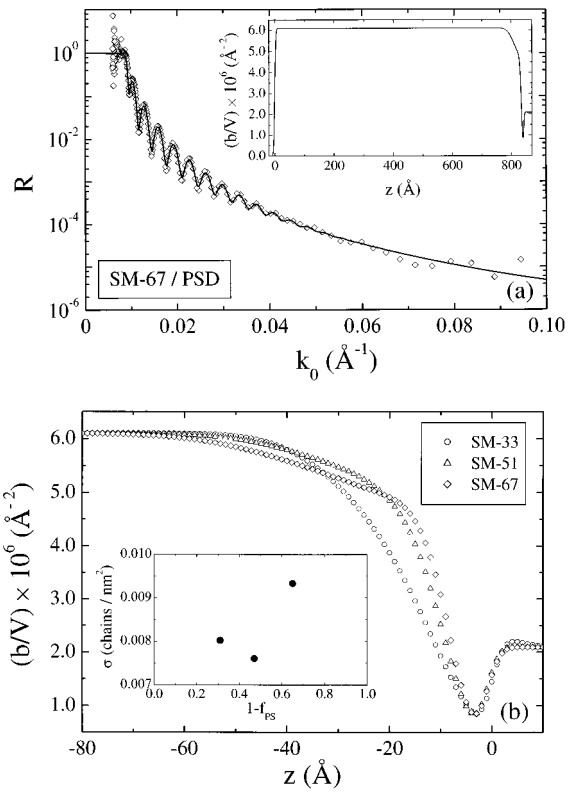

Figure 5. (a) Experimental neutron reflectivity data (◊) as a function of k_0 for a ca. 850 Å thick film of SM-67/PSD. The solid line is the calculated reflectivity curve, convoluted with the appropriate resolution function, using the scattering length density profile shown in the inset ($z = 0$ denotes the air/polymer surface). (b) Scattering length density profiles at the silicon/polymer interface extracted from the analysis of the experimental neutron reflectivity data for all SM/PSD systems: (◊) SM-67/PSD; (△) a ca. 850 Å film of SM-51/PSD; (○) a ca. 900 Å film of SM-33/PSD. The data have been shifted along the z axis so that $z = 0$ denotes the polymer/substrate interface. Inset: The dependence of the surface density of chains σ on the composition of the copolymer in the anchor block, $1 - f_{PS}$, for the SM/PSD systems.

composition changes from 31% anchor to 65% anchor. The profiles have been shifted along the z axis, so that the zero for the polymer/silicon interface is placed at the position where there is the first indication for the substrate. Although the extracted picture in this case is not as clear as in Figure 3, differences in the shapes of the three profiles are evident. Right away, it can be seen that the total adsorbed amounts (proportional to the area above the curves) are different for the three diblocks. Moreover, the extension of the profile toward the bulk homopolymer is also affected by the block-length ratio. The inset of Figure 5b shows the dependence of the surface density of chains σ on the composition of the copolymer in the anchor block (methyl methacrylate), $1 - f_{PS}$. A first observation is that the values of the surface density of chains σ are very low as compared to the SV2P/PSH system. Since PMMA is known to be attracted to the silicon interface almost as much as PV2P, this difference can only indicate that the films were apparently so thin and their concentration was so low that there was not enough copolymer to saturate the interface. Note that no enrichment at the air/polymer interface was observed in any of the SM/PSD systems. The only characteristic of the plot of Figure 5b is a weak increase of the surface density of chains σ as the volume fraction of the anchor increases.

IV. Self-Consistent Mean-Field Theory

IV.1. Introduction. The aim of the present theoretical work is to provide a description of polymer concentrations and conformations in the interfacial region. It utilizes the lattice-based Scheutjens and Fleer[31,32,43] self-consistent field model for multicomponent systems (including block copolymers[5]) as extended to include conformational stiffness.[33,34] This formulation is applied to the case of a mixture of a homopolymer and a diblock copolymer next to a surface.

Polymeric systems are usually characterized by a variety of length scales (i.e., monomers vs entire macromolecules) and, in addition, by conformational and orientational degrees of freedom. A treatment assuming full atomistic description is, in most cases, out of reach of today's computers, or it is still restricted to systems of small sizes and chain lengths. Exact enumeration and Monte Carlo simulations account explicitly for the segments, but are necessarily limited to a small number of chains because of computational limitations. In contrast, methods incorporating a mean field approach can deal with the more realistic situation of a complete ensemble of chains, e.g., the equilibrium between the surface and a bulk phase. On the other hand, due to the large number of possible interactions between macromolecules, the microscopic details average out to a large extent, and it is the chain character and flexibility that determine the main features of their properties. As macromolecules interact with many others, the critical region in which concentration fluctuations become important is very small; the description by means of mean-field approximations is, then, legitimate. Mean-field theories are, thus, widely used to describe inhomogeneous polymeric systems, where the parameters of the model are either derived from a molecular theory or from a comparison with experiments.

Over the past few decades, a substantial effort has been devoted developing mean-field theories, which account for the chain conformational structure. The most powerful one is the self-consistent field approach.[42] This is conveniently implemented on a lattice, where the space is discretized into layers (lattice sites). Although continuum models are more general, it is usually preferred to work with lattice models with the main advantage of a lattice-bond approach being that the infinite number of conformations of real chains in continuum space is reduced to a finite number. Moreover, the average number of interactions is more easily evaluated. Polymer conformations are modeled as random walks on a lattice where the problem of propagation of conformation is usually considered as a first-order Markov process. In such a process, each step or segment "remembers" only the position and orientation of the previous segment. For isolated molecules near a surface, steps toward or within the surface layer are biased with a weighing factor, whereas all other steps are random (i.e., the weighting factor is unity). It is straightforward to extend the one-chain methodology to a many-chain methodology only in the case where one considers independent ideal chains.

To describe properly the thermodynamics of the general macromolecular system, a calculation of the free energy is required. The formulation of the partition function for a dense system on a lattice and the derivation of the free energy from this partition function are rather cumbersome, and many times, it is practically infeasible to derive final expressions for useful physical quantities. Usually it is legitimate to work exclusively with the maximum term of the partition function, ignoring all other terms, which are the source of the fluctuations. In this mean field approximation, each chain is described as feeling the mean field of all surrounding chains. A self-consistent scheme is applied, where the input local concentration produces a local mean field, which is used in order to estimate a new conformational distribution and hence a new value for the local concentration. The scheme is successful when the sequence of approximations for the local density converges.

The most powerful self-consistent mean-field lattice model (SCF) has been derived by Scheutjens and Fleer in order to describe the conformations and concentration profiles of a polymeric system in an interfacial region.[31,32,43] This approach has been used to describe polymer melts and solutions near a solid substrate, polymers chemically attached to the substrate, rings, branched chains, copolymers, multicomponent polymeric systems, and curved interfaces.[32] More recently, the theory has been extended by some of the authors of the present manuscript to incorporate conformational stiffness.[33,34,44] Herein, the theory is applied for the investigation of the adsorption of diblock copolymers to a solid interface from a multicomponent mixture, composed of a polymeric matrix and the diblock. A detailed description of the method and its application in the present system is given in Appendix A.

IV.2. Model Parameters. To perform the calculations, a number of parameters are needed to characterize the specific system under consideration. These are of two types: (a) parameters characteristic of the individual species involved (Flory segment length, bending energy, number of Flory segments), which are obtained from the molecular characterization (molecular weight of the polymers, compositions, as in Tables 1 and 2) and from standard handbooks (bond lengths, bond angles, number of bonds per monomer, molecular weight of the monomer, characteristic ratio, and mass density), and (b) parameters characteristic of the interactions between the various species involved (Flory−Huggins interaction parameter and segment−surface interaction parameters). Moreover, certain experimental quantities from section III are needed, such as film thickness, annealing temperature, and experimental surface excess.

Among the possible choices for the lattice segment size, the ones that have been mostly used are the Kuhn[45] and the Flory segments. In the present study, the model discretization uses a single Flory segment length $\bar{l}_F$, arithmetically averaged over all monomer types. A Flory segment is defined such that a chain will have the same maximally extended length (end-to-end distance in an all-trans conformation) and volume in the Flory segment representation as are measured experimentally.[33] Equating the volume of the Flory chain, containing r Flory segments, to the volume of a real chain, one gets

$$r l_F^3 = \frac{M}{N_{Avog}\rho} = \frac{n_m m}{N_{Avog}\rho} \tag{10}$$

where M is the molecular weight of the chain, ρ its mass density, n_m the degree of polymerization, m the monomer molecular weight, and N_{Avog} the Avogadro number. Moreover, the length of the fully extended Flory chain

is set equal to the maximally extended length of the real chain

$$rl_F = n_b l_b \sin(\theta_b/2) \tag{11}$$

where n_b is the number of chemical bonds per chain, l_b the bond length, and θ_b the bond angle along the chain backbone. Combining eqs 14 and 15, the Flory segment is obtained as

$$l_F = \left[\frac{n_m m}{N_{Avog}\rho n_b l_b \sin(\theta_b/2)}\right]^{1/2} \tag{12}$$

It is noted that the use of Flory segments in the discretization allows correct description of both the chain dimensions and its density. The Flory segment length is commensurate with the spatial resolution of neutron reflectivity experiments.[36−38]

Very important input parameters for the calculation are the surface excesses of the various components, expressed in terms of the layer equivalents Θ_i, defined in Appendix A. For the two blocks of the copolymer, the values of Θ_i are

$$\bar{l}_F\Theta_{PS,c} = z_{PS,c}^* \tag{13a}$$

$$\bar{l}_F\Theta_{anchor} = z_{anchor}^* \tag{13b}$$

where $z_{PS,c}^*$ and z_{anchor}^* are calculated from eqs 2, 8, and 9. Similarly, for the homopolymer matrix

$$\bar{l}_F\Theta_{PS,h} = z_{PS,h}^* \tag{13c}$$

where $z_{PS,h}^* = \int_{interface} \phi_{PS,h}(z)\,dz = \int_{interface} [1 - \phi_{PS,c}(z) - \phi_{anchor}(z)]\,dz$, and thus

$$z_{PS,h}^* = \Lambda - z_{PS,c}^* - z_{anchor}^* \tag{14}$$

where Λ is the total film thickness.

The Flory−Huggins interaction parameters χ between the two different types of segments (styrene and pyridine or styrene and methyl methacrylate) used in the present study are estimated independently of the present experiments. For the polystyrene/poly(methyl methacrylate) system, Fischel and Theodorou[33] estimated $\chi_{PS/PMMA}$ by fitting self-consistent mean-field (SCF) calculations to experimental data[37] for the width of the interface between the respective homopolymers; for the annealing temperature of 170 °C, $\chi_{PS/PMMA} = 0.0463$. For the polystyrene/poly(2-vinylpyridine) system, the SCF calculations are fitted to neutron reflectivity data of the microdomain structure and the interfacial width in an ordered polystyrene-*block*-poly(2-vinylpyridine) diblock copolymer[36] and is presented in Appendix B; for the annealing temperature of 170 °C, $\chi_{PS/PV2P} = 0.1$.

A parametric analysis has been performed with regard to the effective interaction parameters between a polymer segment and a surface site, $\chi_{Si/polymer}$. In the present notation (which follows that of Evers et al.[5]), $\chi_{Si/polymer}$ denotes the energy change (in units of kT) resulting from bringing a polymer segment from pure polymer into an environment of pure substrate and, thus, the adsorption energy is given by $U^a/kT = L\sum_A \phi_A(1)\chi_{Si/A}\lambda_1$; the Silberberg adsorption energy parameter χ_s is related to $\chi_{Si/polymer}$ by $\chi_s = -\lambda_1(\chi_{Si/polymer\ A} - \chi_{Si/polymer\ matrix})$. In the calculations discussed in section V below, $\chi_{Si/PV2P}$ was set to −5 since smaller absolute values gave negligible surface segregation, whereas for larger absolute values the results were practically unaffected. $\chi_{Si/PMMA}$ was also set to −5 but differences were observed for a value of −2, which are discussed in section V. $\chi_{Si/PSD}$ and $\chi_{Si/PSH}$ were set to 0.

Table 3. Model Parameters for PS, PV2P, and PMMA at 170 °C

quantity	units	PS	PV2P	PMMA
m	g/mol	104	103	100
l_b (C−C)	Å	1.54	1.54[a]	1.54
θ_b (C−C−C)	deg	112	112[a]	112
n_{bpm}[b]		2	2	2
ρ	g/cm^3	0.9903	0.9173[c]	1.107
l_F	Å	8.264	8.627	7.664
$\bar{l}_F$	Å	8.445,[d] 7.964[e]	8.445[d]	7.964[e]
n_{mpF}[f]		3.455,[d] 2.897[e]	3.170[d]	3.368[e]
C_∞		10.6	13.0[g]	7.1
l_K	Å	19.7	24.1	13.2
$\epsilon_L/(kT)$		1.055,[d] 0.953[e]	1.341[d]	0.457[e]

[a] Values for PV2P from refs 46 and 47. [b] Number of bonds per monomer $n_{bpm} = n_b/n_m$. [c] Obtained from ref 48 by using the tables at 25 °C and the thermal expansion coefficients therein to estimate values for 170 °C. [d] Values used for the PS/PV2P system. [e] Values used for the PS/PMMA system. [f] Number of monomers per Flory segment $n_{mpF} = n_m/r$. [g] Values for the limit of infinite molecular weight from ref 49 (see formulas and tables therein).

Table 4. Macromolecular Characteristics Used in the SCF Calculations for the PS/PV2P System

code	polymer	$M_{w,i}$ (g/mol)	$n_{m,i}$	r^i	$\langle R_g^2\rangle_i^{1/2}$ (Å)[a]	$\langle R^2\rangle_i^{1/2}$ (Å)[b]	L_i (Å)[c]
all	PSD	75 000	670	194	75	183	1711
SV2P-3.4	PV2P	3400	32	10	17	42	82
SV2P-18	PV2P	18 000	171	54	42	102	437
SV2P-32	PV2P	32 000	305	96	56	136	779
SV2P-45	PV2P	45 000	429	135	66	162	1095
SV2P-68	PV2P	68 000	648	204	81	199	1655
SV2P-95	PV2P	96 000	914	288	97	237	2334
SV2P-102	PV2P	102 000	971	306	100	244	2479
PS,h	PSH	186 000	1788	518	122	300	4566

[a] Root mean-square unperturbed radii of gyration. [b] Root mean-square unperturbed end-to-end distance. [c] Maximally extended length of a real chain.

Table 5. Macromolecular Characteristics Used in the SCF Calculations for the PS/PMMA System

code	polymer	$M_{w,i}$ (g/mol)	$n_{m,i}$	r^i	$\langle R_g^2\rangle_i^{1/2}$ (Å)[a]	$\langle R^2\rangle_i^{1/2}$ (Å)[b]	L_i (Å)[c]
SM-67	PSH	115 200	1108	382	96	236	2829
SM-51	PSH	87 200	838	289	84	205	2140
SM-33	PSH	57 800	555	192	68	167	1417
SM-67	PMMA	56 800	568	169	56	138	1450
SM-51	PMMA	83 800	838	249	68	168	2140
SM-33	PMMA	117 200	1172	348	81	198	2993
PS,h	PSD	204 000	1821	629	123	302	4650

[a] Root mean-square unperturbed radii of gyration. [b] Root mean-square unperturbed end-to-end distance. [c] Maximally extended length of a real chain.

V. Modeling Results and Discussion

Self-consistent mean-field calculations have been performed with the model presented in section IV with its details in Appendix A. The calculations were performed for exactly the same systems investigated experimentally by neutron reflectivity using the molecular parameters of Table 3. Tables 4 and 5 list the macromolecular characteristics of all the polymers in the parameter space used in the calculations.

Figure 6a shows the theoretical volume fraction profiles of all species near the silicon interface for a film

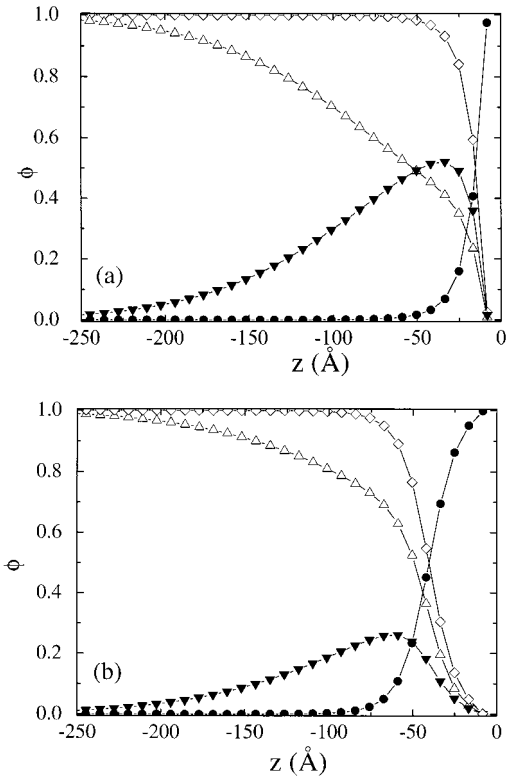

Figure 6. Theoretical volume fraction profiles for all species near the silicon interface for (a) SV2P-18/PSH and (b) SV2P-95/PSH: (●) the anchor PV2P block; (▼) the dangling PSD block; (△) the homopolymer PSH; (◊) the profile of the total polystyrene (sum of the PSD and PSH).

wherein the copolymer has a relatively short pyridine block, i.e., for SV2P-18/PSH. $\phi_{PV2P} = \phi_{anchor}$ refers to the anchor PV2P block, $\phi_{PSD} = \phi_{PS,c}$ to the dangling PSD block, $\phi_{PSH} = \phi_{PS,h}$ to the homopolymer PSH, whereas $\phi_{PS} = \phi_{PSD} + \phi_{PSH} = \phi_{PS,c} + \phi_{PS,h}$ is the profile of the total polystyrene (sum of the PSD and PSH). The lengths in the calculations were expressed in Flory segments and are translated to angstroms using the value of $\bar{l}_F = 8.445$ Å. The pyridine block is adsorbed at the silicon interface (as expected) and extends to only a few Flory segments away from the interface. The deuterated polystyrene block forms the dangling tail, with its profile exhibiting a depletion near the wall and a maximum of about 50% at a distance of a few Flory segments from the interface. Moreover, the polystyrene homopolymer is pushed away from the wall, almost being excluded from the interfacial region.

Figure 6b shows the respective theoretical volume fraction profiles near the silicon interface for a film wherein the copolymer has a long pyridine block, i.e., for SV2P-95/PSH. Significant differences are observed in relation to the SV2P-18/PSH film of Figure 6a. The pyridine block, adsorbed at the silicon interface, now extends significantly farther away from the interface. Moreover, the shape of the profile of the dangling deuterated polystyrene block is different: it exhibits a wide depletion near the wall and a maximum of only about 25%, which is shifted away from the interface relative to Figure 6a. The polystyrene homopolymer is, thus, not so much excluded from the interfacial region, whereas the total polystyrene vs PV2P profile exhibits an interfacial width that is comparable to that between the two blocks in an ordered diblock copolymer[36] (see also Appendix B), which, in a different system, was found to be the same as that between the respective homopolymers.[37]

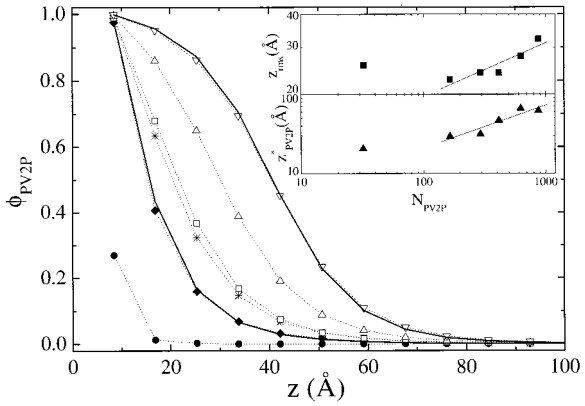

Figure 7. Theoretical volume fraction profiles of the anchoring pyridine block at the silicon/polymer interface calculated for all SV2P/PSH systems: (●) SV2P-3.4; (♦) SV2P-18; (∗) SV2P-32; (□) SV2P-45; (△) SV2P-68; (▽) SV2P-95. Upper inset: root-mean-square thickness of the pyridine layer vs N_{PV2P}. Lower inset: adsorbed amount of pyridine vs N_{PV2P}. Both axes in the insets are logarithmic. The thick lines in the main Figure show the theoretical volume fraction profiles of PV2P homopolymer for films of PV2P/PSH mixtures (the molecular weight of the PV2P homopolymer is equal to that of the block of the SV2P for SV2P-18 and SV2P-95) at the same adsorbed amount of pyridine segments.

The profile of the anchoring block is intriguing, since it is usually thought that the anchor would form a flat (pancakelike) layer at the interface with a width of a few segments, independently of its molecular weight. It is noted, however, that those statements were made basically for block copolymers adsorbed onto a solid surface from solution,[6,9,10] where the different interactions between the anchor and the solvent may indeed modify the conformation of the anchor. For diblock copolymers adsorbed from the melt, the present calculations show clearly a thickening of the profiles of the anchor block $\phi_{PV2P} = \phi_{anchor}$ as the molecular weight $N_{PV2P} = N_{anchor}$ increases; this is shown in Figure 7 for the series of SV2P/PSH systems investigated. Calculation of the root-mean-square thickness of the anchor, $z_{rms} = \langle z_{anchor}^2 \rangle^{1/2} = \int_{interface} \phi_{anchor}(z) z^2 \, dz / \int_{interface} \phi_{anchor}(z) \, dz$, results in a $N_{PV2P}^{0.2}$ dependence (upper inset of Figure 7) for the all anchor molecular weights except for the lowest (SV2P-3.4). It is evident that more experiments are required to cover the regime between the two lowest PV2P molecular weights, i.e., between SV2P-3.4 and SV2P-18. Moreover, the dependence of the surface excess of PV2P, $z_{PV2P}^* = z_{anchor}^*$, on the PV2P molecular weight (lower inset of Figure 7) conforms to a $N_{PV2P}^{0.54}$ dependence (excluding SV2P-3.4). It is noted that the exponents above should be viewed with caution since the ordinates cover a very limited range.

To further investigate the shape of the anchor profile, calculations were performed for the volume fraction profiles near the silicon interface for mixtures of PV2P with polystyrene. The comparison between the volume fraction profiles of the PV2P block for SV2P/PSH films with those for PV2P/PSH films (the molecular weight of the PV2P homopolymer is equal to that of the block of the SV2P) at the same adsorbed amount of pyridine segments is also shown in Figure 7 with the thick solid lines for PV2P-18 and PV2P-95: for both systems, the two profiles are indistinguishable. Therefore, the profile of the anchoring block should be thought of as being

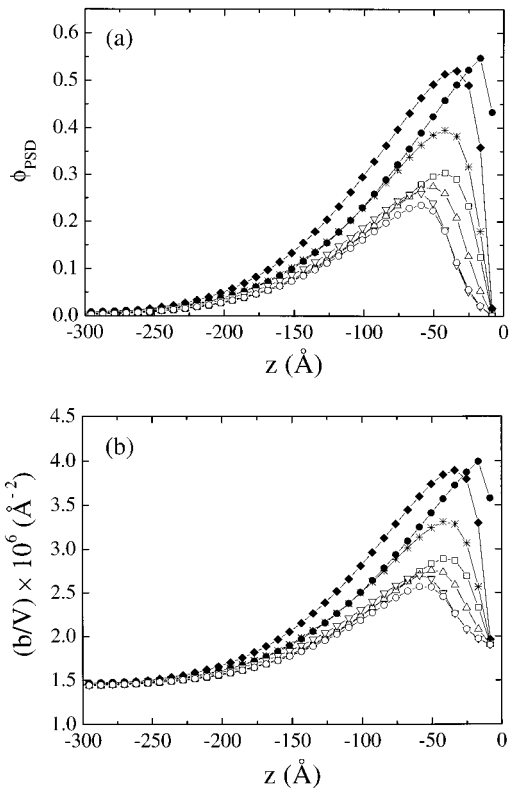

Figure 8. Theoretical results for (a) the volume fraction profiles of the dangling styrene block and (b) the scattering length density profiles at the silicon/polymer interface calculated for all SV2P/PSH systems: (●) SV2P-3.4; (♦) SV2P-18; (∗) SV2P-32; (□) SV2P-45; (△) SV2P-68; (▽) SV2P-95; (○) SV2P-102.

identical to that of a physically adsorbed homopolymer from the same matrix to the same interface (it is noted that for the lowest molecular weight SV2P-3.4 the above statement does not precisely hold). If one thinks that PV2P is in a "bad" solvent, then its dimensions should show a $N_{PV2P}^{1/3}$ dependence, whereas for a pancake, a N_{PV2P}^{0} dependence was envisioned. The $N_{PV2P}^{0.2}$ behavior observed is between these two limits. It is noted that the only other time that the similarity of the shape of the anchor to that of a physically adsorbed homopolymer has been suggested was in the study of Evers et al.[5] for diblocks adsorbed from solution, whereas all other studies consider the anchor as forming a very thin (pancakelike) layer of constant thickness of a few nanometers.[6,9,10] The present experiments only indirectly probe the profile of the anchor, which indeed appears to become broader as the anchor molecular weight increases (Figure 3). The experiments on the SM/PSD systems cannot provide any more information on this, since both copolymer blocks are hydrogenous. Experiments are planned on SV2P/PSD systems (with both the dangling polystyrene and the homopolystyrene deuterated). However, since the scattering length of PV2P is very similar to that of the substrate, the interpretation of the data is not expected to be without ambiguities. A better experiment would utilize a deuterated anchor block.

One can now return to the shapes of the volume fraction profiles of the dangling blocks as a function of the molecular weight of the anchor. Figure 8a shows the $\phi_{PSD} = \phi_{PS,c}$ volume fraction profiles for the series of SV2P/PSH systems investigated. The calculations show a behavior consistent with the discussion of SV2P-18 and SV2P-95 in Figure 6, parts a and b. The profiles for the two shorter PV2P blocks exhibit a sharp depletion layer near the substrate and a high maximum (about 50%), whereas those for the four longer PV2P show a wide depletion layer and a maximum of only about 20−30%. The data for SV2P-32 clearly fall between the two regimes. For a better comparison with the experimental data, the volume fraction profiles of all the species present were used to estimate the theoretical scattering length density profiles (b/V) vs z using eq 5. These contain less information than Figures 6a,b and 8a but allow for a direct comparison with the experimental data. The calculated scattering length density profiles are shown in Figure 8b for all the SV2P/PSH systems. The qualitative agreement with the experimental data in Figure 3 is evident.

Even more significant, however, is the very good agreement on the N_{PV2P} dependence of the quantities z_{max} and $(b/V)_{max}$ estimated from the theory with those estimated from the analysis of the experimental data; this comparison is shown in Figure 4. The characteristic change in the behavior of these quantities between that for low N_{PV2P} and that for high N_{PV2P} is also evident in the calculations. The position of the maximum of the (b/V) profile, z_{max}, moves away from the surface as N_{PV2P} increases for low values of N_{PV2P}, whereas it is almost insensitive to N_{PV2P} for higher values (some difference is noted for SV2P-45, for which the experimental z_{max} has already reached the plateau, whereas the theoretical has not). The quantitative difference between the experimental and theoretical z_{max} for all samples is believed to be due to the uncertainties in the positioning of the polymer/substrate interface, which was necessary in order to construct Figure 3. Note that, as discussed in reference to Figure 4, the shift of the position of the maximum is partially due to the widening of the profile of the anchor. However, as was shown in Figure 7, this widening of the PV2P profile is continuous and, thus, if, this was the only factor involved, z_{max} would continuously increase and would not show the behavior of the experimental points in Figure 4a. The theoretical maximum scattering length density $(b/V)_{max}$ shows the "transition" from high values at low N_{PV2P} toward low values for high N_{PV2P}, whereas the agreement with the experiment is quantitative. Note that it is not fair to compare the values for the surface excess of the dangling block, z_{PSD}*, or, equivalently, the surface density of copolymer chains, σ, since this is more-or-less an input to the calculations. Once more, it is stated that the change in the behavior of z_{max}, $(b/V)_{max}$, and z_{PSD}* or σ can only be due to a change in the configuration of the dangling block between low and high values of N_{PV2P}; however, it is apparent that the transition from a "brush"-like configuration at low values of N_{PV2P} (higher σ) toward a "mushroom"-like configuration at high values of N_{PV2P} (low σ) is a smooth one.

Before finishing with the results of the SCF calculations for the SV2P/PSH system, one would like to present some more information on the internal characteristics of the various profiles, which cannot easily be extracted from experiment. Such pieces of information relate to the distribution of the copolymer junctions and end segments within the interfacial film. The profile of the copolymer junctions provides another measure of the width of the interfacial region. The volume fraction of a junction is defined as the arithmetic mean of the volume fractions of the PS and the PV2P segments

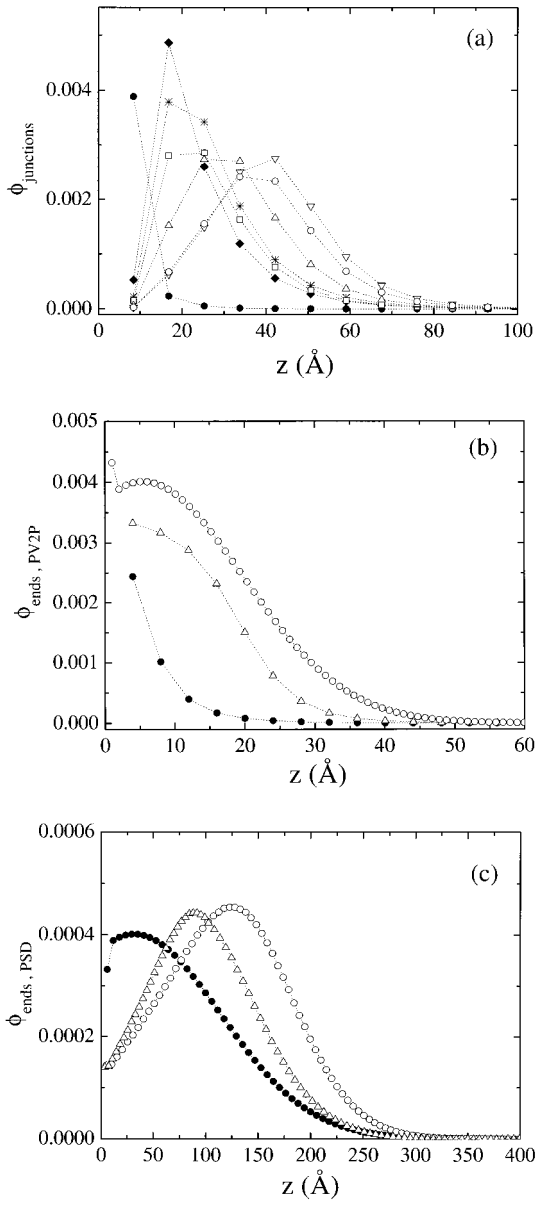

Figure 9. Theoretical results for (a) the profiles of the copolymer junctions, (b) the end-segment distributions for the free ends of the anchor PV2P, and (c) the end-segment distributions for the free ends of the dangling PSD blocks of the copolymer for the SV2P/PSH systems: (●) SV2P-3.4; (♦) SV2P-18; (∗) SV2P-32; (□) SV2P-45; (△) SV2P-68; (▽) SV2P-95; (○) SV2P-102.

connected at the junction. These profiles are shown in Figure 9a for all the SV2P/PSH films. It is observed that the junction profiles exhibit a moderate maximum (except for sample SV2P-3.4 with the lowest molecular weight of the PV2P block). The full-width at half-maximum increases as the N_{PV2P} increases. For the largest PV2P molecular weight (i.e., for SV2P-102), the full-width at half-maximum has a value close to the experimental value for the interfacial width of the PS−PV2P system.[36] Moreover, for all samples except SV2P-102, the junction profiles are rather asymmetric, with a tail extending away from the substrate.

The end-segment distributions for the free ends of the anchor PV2P and of the dangling PSD blocks of the copolymer are shown in Figure 9, parts b and c, respectively, for three samples: SV2P-3.4/PSH, SV2P-68/PSH, and SV2P-102/PSH. The profiles of the end segments of the PV2P block are consistent with the profiles shown in Figure 7; the maximum occurs very close to the substrate for all molecular weights. In contrast, the free ends of the dangling PSD chains are distributed more freely within the interfacial layer and are not restricted to within the outer region of the adsorbed layer, as would have been expected for an Alexander−de Gennes brush,[25] rather in accord with the predictions of Semenov[50] in the melt or the analogous prediction in solution.[51]

One can now discuss the SM/PSH system. As also discussed in section III, the analysis of the experimental data in this case is less unambiguous, due to the contrast of the various components for the neutrons. It is noted that in the experiment both copolymer blocks were hydrogenous (with scattering length densities not so different from the silicon substrate) whereas the matrix was deuterated. Besides, the estimated scattering length density profiles lead to very low values for the surface density of chains σ (Figure 5). Moreover, this system is different from the SV2P/PSD one, since the total molecular weights of the (three) copolymers are almost the same, whereas their composition varies from 0.31 to 0.65 anchor; this means that both the molecular weight of the anchor and of the dangling chain are different among the three samples. Thus, the SCF calculations are very important for one to shed light on the chain conformation.

The volume fraction profiles of the anchor PMMA and of the dangling PSH blocks are shown in Figure 10, parts a and b, respectively, for the three SM/PSD films, whereas Figure 10c shows the calculated scattering length density profiles estimated from transforming the volume fraction profiles using eq 5 with $(b/V)_{PS,c} = (b/V)_{PSH} = 1.43 \times 10^{-6}$ Å^{-2}, $(b/V)_{anchor} = (b/V)_{PMMA} = 1.0 \times 10^{-6}$ Å^{-2}, and $(b/V)_{PS,h} = (b/V)_{PSD} = 6.1 \times 10^{-6}$ Å^{-2}. It is also noted that the calculations again have been performed using as input the total surface excess of the diblock z^* (or, equivalently, the surface density of copolymer chains σ), which was estimated from the neutron reflectivity data (eqs 4, 7, and 9). The shapes of the profiles are in general similar to those of the SV2P/PSH system of similar compositions, keeping in mind the much lower surface excess. As the anchor molecular weight increases, the PMMA layer becomes thicker, as was observed for the respective case of PV2P. For example, SM-51 (containing $N_{PS,c} = N_{PSH} = 890$ and $N_{anchor} = N_{PMMA} = 790$) can be thought of as analogous to SV2P-68 (containing $N_{PS,c} = N_{PSD} = 750$ and $N_{anchor} = N_{PV2P} = 623$), whereas SM-33 (containing $N_{PS,c} = N_{PSH} = 592$ and $N_{anchor} = N_{PMMA} = 1098$) as analogous to SV2P-102 (containing $N_{PS,c} = N_{PSD} = 750$ and $N_{anchor} = N_{PV2P} = 935$). Comparison of Figures 7 and 10a show similar behavior. However, certain differences associated with the shape of the PS blocks (Figure 8a and 10b) can be noted in comparing the above two pairs of systems. The maximum values of the volume fractions of the dangling PS blocks occur at distances shifted to lower values compared to those of the SV2P system. This should be expected, since the Flory−Huggins interaction parameter between the unlike segments is different, i.e., much larger for SV2P than for SM; thus, the PS blocks of the SV2P copolymer extend more in order to minimize the contacts with the PV2P block. Moreover, a parametric analysis was performed with regard to the interaction between silicon and PMMA, $\chi_{Si/PMMA}$. The calculation compares somehow better with

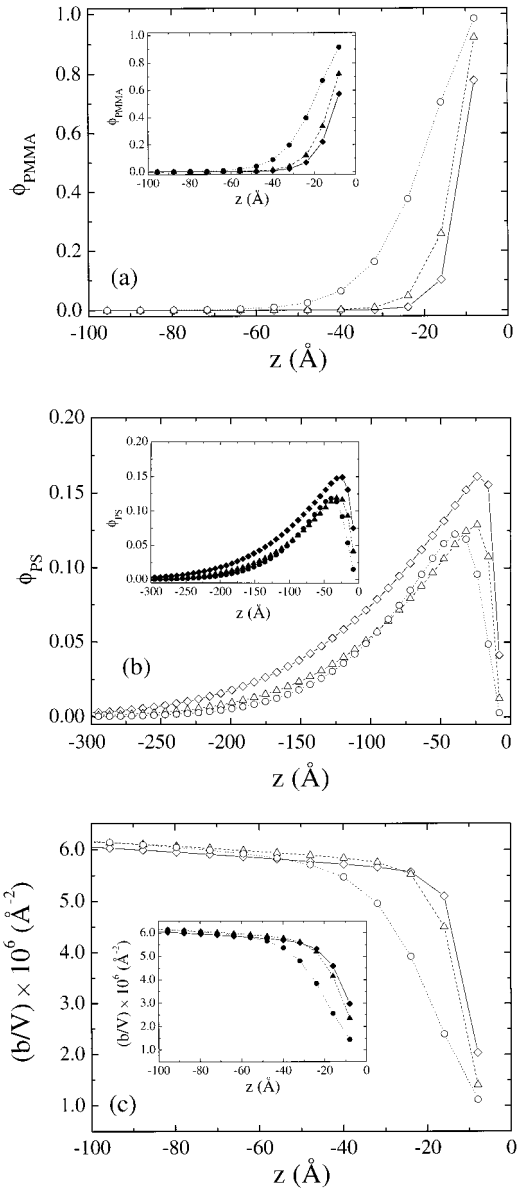

Figure 10. Theoretical results for (a) the volume fraction profiles of the anchor PMMA, (b) the volume fraction profiles of the dangling PSH blocks, and (c) the scattering length density profiles at the silicon/polymer interface calculated for the three SM/PSD films: (○) SM-33; (△) SM-51; and (◇) SM-67. In the insets, the respective profiles are shown for $\chi_{Si/PMMA} = -2$ for the three samples (filled symbols).

the data for lower strength (in absolute value) of the interaction between the surface and the adsorbed polymer, e.g., for $\chi_{Si/PMMA} = -2$ shown in the insets of parts a−c of Figure 10. When the interaction between the surface and the polymer is lowered (in absolute value), the shape of the profile of the anchor block becomes broader whereas there are negligible changes in that of the tail. Moreover, it is the sample with the smallest molecular weight of the anchor (SM-67) that is affected the most. However, the very low surface densities (Figure 5b) do not permit any further discussion on the strength of the substrate/polymer interactions.

It is noted that the data and the theoretical analysis for the SM/PSD system do not give any new information than what was estimated from the SV2P/PSH system. However, they are consistent with the former, and thus, they are useful. As noted in the Experimental Section, it is believed that the much lower adsorbed amount in the SM/PSD system is not related to any significant difference in the physicochemical characteristics of the system but rather to the fact that the films were made very thin and with lower concentration, and thus, it was not possible to achieve full coverage of the surface. Experiments are underway to quantitatively examine the dependence of the shape of the profiles on the film thickness (or on the ability to saturate the surface).

IV. Concluding Remarks

The segment density profiles of the adsorbed diblock copolymers for thin copolymer/homopolymer films have been investigated experimentally by neutron reflectivity and theoretically using a lattice-based self-consistent field model inspired by the work of Scheutjens and Fleer, as extended to incorporate chain conformational stiffness. The theory uses as inputs the molecular and macromolecular characteristics of the various polymers and their interactions as well as the experimental data on total surface excess. The aim of the work was to probe the changes in the adsorbed chain configuration as a function of the block-length ratio of the diblocks. Utilizing a series of diblocks with the same molecular weight of the dangling block and different molecular weights of the anchoring block (from much smaller to much larger than the tail block) evidence is presented for the existence of a "mushroom", a "wet brush", and a broad transition regime regarding the configuration of the dangling chains. An investigation using a series of diblocks with constant total molecular weight and different compositions lead to consistent (although not as clear) results.

Investigations are underway to study the effects of additive concentration and film thickness on the dangling chain conformation. Besides, it is noted that, in the present investigation as well as in almost all previous studies, the possibility of an interaction (either repulsive or attractive) between the dangling chains and the matrix homopolymer has been neglected. Aubouy and Raphaël[29] showed that even very weak repulsive interactions may lead to new regions in the various scaling regimes. It is, therefore, planned to investigate the dangling chain conformations and their changes for systems where such interactions are present.

Acknowledgment. We would like to acknowledge that part of this research was sponsored by NATO's Scientific Affairs Division in the frameworks of the Science for Stability and Science for Peace Programmes and by the Greek General Secretariat of Research and Technology (ΠΕΝΕΔ Programme, 99ΕΔ23). This work was supported (in part) under the auspices of the United States Department of Energy. The Manuel Lujan, Jr., Neutron Scattering Center is a national user facility funded by the Office of Basic Energy Sciences, Materials Science, United States Department of Energy, under Contract Number W-7405-ENG-36 with the University of California. We would like to thank Dr. P. van Huten for his early data reduction and analysis.

Appendix A

The system considered is an equilibrated, multicomponent melt next to solid surface. The system is discretized into a three-dimensional (*xyz*) lattice of simple

cubic symmetry with full occupancy. The substrate is placed parallel to the *xy* plane with the resulting lattice layers of the polymer (planes parallel to the surface) numbered consecutively $z = 1, 2, ...$, starting from the layer next to the surface ($z = 1$). In this work (for computational convenience), two walls are assumed at $z = 0$ and $z = M + 1$ where the presence of the substrate has negligible effects at the mid-layers ($z = M/2$). Each layer has a thickness of a Flory segment length l_F, and contains L_F lattice sites. Each lattice site has Z neighboring sites, a fraction λ_0 of which lie in the same layer and a fraction λ_1 lie in each of the adjacent layers, where $\lambda_1 + \lambda_0 + \lambda_1 = 1$. The coordination number Z reflects the point symmetry characterizing the lattice (for a cubic lattice: $Z = 6$, $\lambda_0 = {}^4/_6$ and $\lambda_1 = {}^1/_6$). To describe a system of constant volume, each lattice site has to be occupied by exactly one segment. A polymer molecule is represented by a chain of r^i connected segments, numbered $s = 1, 2, ..., r^i$ (index i denotes the type of the molecule). Each chain has a defined chemical sequence (for example ...AAAAABBB...), with the type of segment s designated by $t_i(s)$ (=A, B, ...), and contains $r_A{}^i$ segments of type A, i.e., $r_A{}^i = \sum_{s=1}^{r^i} \delta_{A,ti}(s)$; each segment (independently of the segment type) occupies the same volume, equal to that of the lattice site, $l_F{}^3$. The total number of chains of type i in the lattice is given by $n_i = \sum_{z=1}^{M} L_F \phi_i(z)/r^i \equiv L_F \Theta_i/r^i$, where Θ_i is the number of *layer equivalents* of component type i.

Each chain can assume a large number of possible conformations in the lattice. Each conformation (c) is defined by specifying the layer numbers in which each of the successive chain segments finds itself (i.e., $c \equiv \{(s = 1, z = z_1), (s = 2, z = z_2), ..., (s = r_J{}^i, z = z_{rJ^i})\}$, $J =$ A, B, ...). The number of chains i in conformation c is indicated as $n_i{}^c$. The chains are distributed over the various possible configurations (sets of conformations $\{n_i{}^c\}$) in the lattice with statistical weights depending on the energy and entropy of each configuration. The proper description of the system is given in the context of statistical physics by means of the grand canonical partition function. The nonbonded chain interactions are approximated using the Bragg-Williams mean field approximation and the intrachain interactions are approximated using bending energies. The counting of the number of ways of arranging chains over available sites is readily performed on a lattice model. Equilibrium is the state at which the chains are distributed over the various possible conformations in the lattice such that the free energy (derived from the partition function) is at its minimum. The assumption is made of replacing the sum of several terms in the partition function by its maximum term (i.e., zero fluctuations of the density in the (xy) directions). To obtain an expression for the number of molecules $n_i{}^c$ of chain type i of size r^i in conformation c, the natural logarithm of the maximum term of the partition function is minimized with respect to $n_i{}^c$, subject to the full occupancy constraint applied layer-wise. It was shown[33,34] that one can describe the system in a mean field self-consistent approximation in terms of a segment potential $u_A(z)$, which depends only on the chemical nature of the segment. Equivalently, a description can be given in terms of a segment weighting factor, $G_A(z) = \exp[-u_A(z)/(kT)]$, where kT is the thermal energy. The weight $G_A(z)$ is proportional to the probability of finding a type-A segment in layer z of the interfacial system relative to finding it in the bulk. Values of $G_A(z)$ very close to unity (for a given layer z) indicate that the effect of the substrate at layer z is negligible.

In the modified version of the SCF theory,[33,34] conformational stiffness is introduced by assigning different bending energies to different bending angles formed by triplets of segments. For a cubic lattice only 0° (back folding or V conformer), 90° (L conformer), and 180° (straight or I conformer) bending angles are possible. The two consecutive segments define a bond b. In a cubic lattice the z-projection of a bond, reduced by the lattice constant, has three values: for two consecutive segments lying in layers z and $z + 1$, $b = +1$; for two consecutive segments lying in layers z and $z - 1$, $b = -1$; $b = 0$ if both consecutive segments lie within layer z. Thus, b (of segment s) $\equiv b(s) = z_s - z_{s-1}$. The bending energies associated with each of these conformations are denoted by ϵ_V, ϵ_L, and ϵ_I (more generally, ϵ_{b_{s-1},b_s}) with corresponding Boltzmann factors $\tau_V = \exp[-\epsilon_V/(kT)]$, $\tau_L = \exp[-\epsilon_L/(kT)]$ and $\tau_I = \exp[-\epsilon_I/(kT)]$, respectively or, more generally, $\tau^{i;s}_{b_{s-1},b_s}$ (i denotes the chain type).

The bending energies can be determined from the characteristic ratios C_∞,[33] by matching the mean-square end-to-end distance between a real chain and a chain of correlated Flory segments

$$\langle R^2 \rangle = C_\infty n_b l_b{}^2 = C_\infty^F (r - 1) l_F{}^2 \qquad \text{(A1)}$$

where C_∞ is the characteristic ratio of the real chain and C_∞^F the characteristic ratio of the correlated Flory chain. Assuming that $\tau_V = 0$ (i.e., back-folding is forbidden), the characteristic ratio of the Flory chain is related to the bending statistical weights by[33]

$$C_\infty{}^F = 1 + \frac{\tau_I}{2\tau_L} = 1 + \frac{1}{2}\exp\left(\frac{\epsilon_L - \epsilon_I}{kT}\right) \qquad \text{(A2)}$$

Moreover, since the characteristic ratio depends only on the difference between the energies ($\epsilon_L - \epsilon_I$), one may set one arbitrarily to zero (herein $\epsilon_I = 0$). Thus, the bending energy ϵ_L can be estimated from eqs A1 and A2 if the values of C_∞ of the homopolymers is known. The junction bending energies of copolymers are approximated as the arithmetic averages of the bending energies of the segment types involved in the junction. The values for all the above parameters, which are used in the calculations presented in section V, are given in Table 3 for both systems investigated.

In the present formulation, initially introduced by Fischel and Theodorou,[33] a second-order Markov process is considered, where an end-segment statistical weight $G_i{}^{b_s}(z,s|1)$ is introduced for the specification of two segment positions ($s - 1$ and s): this is the statistical weight of a chain portion consisting of segments 1, 2, ..., s of a chain of type i for which segment s is in layer z, segment ($s - 1$) is in layer ($z - b_s$) and the positions of all the other segments of that chain are summed over all possibilities. Moreover, one can define $G_i(z,s|1)$, without the index for the bond, as $G_i(z,s|1) = \sum_{b_s} G_i{}^{b_s}(z,s|1)$. These weights follow a recursion relation[33,34]

$$G_i{}^{b_s}(z,s|1) = G_i(z,s)\lambda_{|b_s|} \sum_{b_{s-1}} \tau^{i;s}_{b_{s-1}b_s} G_i{}^{b_{s-1}}(z - b_s, s - 1|1) \qquad \text{(A3)}$$

where $G_i(z,s)$ is the segment weighting factor for segment s of chain of type i to be in layer z (it equals $G_A(z)$ when $A = t_i(s)$). The bending energy contribution[44] of

each possible combination of a pair of successive bonds (b_{s-1},b_s) is properly weighted through the factor $\tau^{i;s}_{b_{s-1}b_s}$, which depends on the chain type i, and on the position of the segments $s-1$, s, and $s+1$. The recursion relation (eq A3) describes forward propagation (from segment 1 to segment s). An analogous recursion relation describes backward propagation (from segment r^i to segment s):

$$G_i^{b_{s+1}}(z, s|r^i) = G_i(z,s)\lambda_{|b_{s+1}|}\sum_{b_{s+2}}\tau^{i;s}_{b_{s+1}b_{s+2}}G_i^{b_{s+2}}(z + b_{s+1}, s + 1|r^i) \quad \text{(A4)}$$

The initial values can easily be guessed as $G_i^{b_s}(z,1|1) = G_i(z,1)/3$ for the forward propagation and $G_i^{b_{r^i}i+1}(z,r^i|r^i) = G_i(z,r^i)/3$ for the backward propagation. To be able to apply the recursion relation (eq A3) throughout the system, one needs to define the bonds b_1 $(=z_{s=1} - z_{s=0})$ and b_{r^i+1} $(=z_{s=r^i+1} - z_{s\,=\,r^i})$. In that case, a "ghost" segment $s = 0$ is introduced,[34] where it is quite legitimate to assume that the three possible conformations (I, L, and V) in which the "ghost" segment is involved carry the same bending energy for any chain type; hence the respective Boltzmann factors are equal $(\tau_V^{i;s=0} = \tau_L^{i;s=0} = \tau_I^{i;s=0} = {}^1/_3)$. Similarly, a "ghost" segment is added at the other end of the chain in order to define bond b_{r^i+1} and thus extend the applicability of the backward recursion relation up to the segment just before the last segment.

The volume fractions for a specific chain type are found using the "connectivity law" or "composition law"[33]

$$\phi_i(z) = C_i\sum_{s=1}^{r^i}\sum_{b_s}\sum_{b_{s+1}}\frac{G_i^{b_s}(z,s|1)\tau^{i;s}_{b_{s-1}b_s}G_i^{b_{s+1}}(z, s|r^i)}{G_i(z,s)} \quad \text{(A5)}$$

The "composition law" expresses how the volume fractions depend on the statistical weights, and hence, on the segment potential. If the total amount Θ_i of molecule i is known, the normalization constant, C_i, is directly obtained from

$$C_i = \frac{\Theta_i}{r^i G_i(r^i,1)} \quad \text{(A6)}$$

where $G_i(r^i,1) = \sum_z \sum_{b_{ri}} G_i^{b_{r^i}}(z,r^i|1)$.

The segment potential profiles are calculated self-consistently using a numerical method initially developed by Evers et al.[5] and modified[33,34] in order to incorporate chain stiffness. In this numerical method a set of coupled nonlinear equations is solved by the Powell method.[52] During the solution of the equations, it is taken into account that the segment potential has an excluded volume part, which is independent of the segment type, whereas the full occupancy condition, $\sum_i \phi_i(z) = 1$, is assumed for every layer z.

Appendix B

The Flory−Huggins interaction parameters χ between the two different types of segments (styrene and pyridine or styrene and methyl methacrylate) used in the present study are estimated independently of the present experiments by investigating simpler systems.

For the polystyrene/poly(methyl methacrylate) system, Fischel and Theodorou[33] estimated $\chi_{PS/PMMA}$ by matching the width of the interface between the respective homopolymers estimated from the self-consistent mean-field (SCF) model with experimental neutron reflectivity data;[37] this gave $\chi_{PS/PMMA} = 0.0463$ for the annealing temperature of 170 °C within the present definition of a Flory segment. Note that capillary waves and their influence on the experimental interfacial widths were not considered explicitly in the one-dimensional SCF model treatment; their effect is absorbed into the value of the fitted parameter χ. Although this may lead to values of the effective χ, which are much different from those estimated by other methods (0.0372 for that system[37,53]), use of the present estimates was adequate to describe the structure and thermodynamics of the interface between PS and PMMA in the absence and in the presence of a PS−PMMA diblock at the interface.

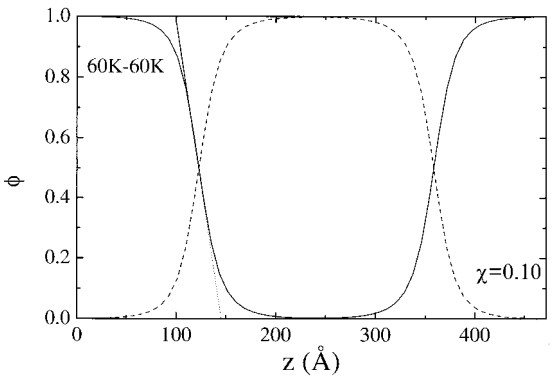

Figure 11. SCF calculations on a PS−PV2P 60−60 ordered diblock copolymer film: volume fraction profiles of both styrene (dashed line) and pyridine (solid line) along one period of the ordered microdomain morphology calculated for $\chi_{PS/PV2P} = 0.1$. For this value of $\chi_{PS/PV2P}$ the interfacial width is 45 Å, in agreement with experimental data.[36] The dotted line is a guide for the evaluation of the interfacial width.

To estimate the interaction parameter for the polystyrene/poly(2-vinylpyridine), $\chi_{PS/PV2P}$, SCF calculations were performed for a thin film of an ordered (pure) poly(2-vinylpyridine)-*block*-polystyrene diblock copolymer investigated by Anastasiadis et al.[36] The diblock was PS−PV2P 60−60 with characteristics $M_n = 100\,000$, $M_w = 108\,000$, $N_{total} = 996$, and $f_{PS} = 0.465$ annealed at 170 °C. The surface induced orientation of the copolymer microdomains parallel to the free and the substrate interfaces allowed the investigation of the morphology by neutron reflectivity, which gave an interfacial width $a_I = 45 \pm 3$ Å (when fitted with a hyperbolic tangent profile) and a long period $L_{cop} \equiv L_{PS} + L_{PV2P} = 536 \pm 4$ Å.

SCF calculations were performed on a ∼1900 Å film of PS−PV2P 60−60 using the molecular parameters of Table 3 and treating $\chi_{PS/PV2P}$ as an adjustable parameter. Figure 11 shows the volume fraction profiles of both styrene and pyridine along one period of the ordered microdomain morphology calculated for $\chi_{PS/PV2P} = 0.1$. For this value of $\chi_{PS/PV2P}$, the calculated interfacial width was 45 Å, i.e., equal to the experimental value.

Moreover, to test the credibility of the SCF approximation, the long period of the lamellar diblock was investigated. Figure 12 shows the calculated Helmholtz free energy as a function of the long period of the diblock for $\chi_{PS/PV2P} = 0.11$ and $\chi_{PS/PV2P} = 0.10$ (with and without considering the influence of chain stiffness). The free energy is calculated with reference (usually denoted by $*$) to a state where the molecules of each component are in independent, homogeneous, pure phases (a hypo-

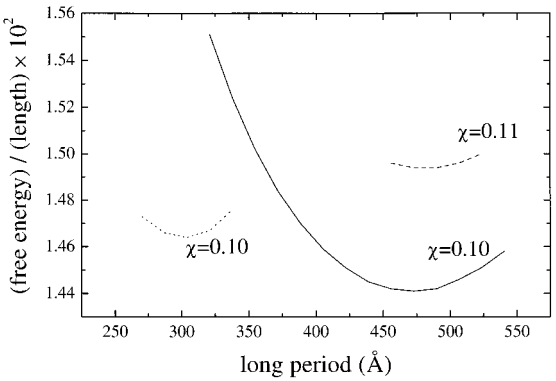

Figure 12. Calculated Helmholtz free energy as a function of the long period of the PS−PV2P 60−60 diblock for $\chi_{PS/PV2P} = 0.10$ (solid line) and $\chi_{PS/PV2P} = 0.11$ (dashed line) including the modification due to chain stiffness, whereas the dotted line is the calculation for $\chi_{PS/PV2P} = 0.10$ without considering the influence of chain stiffness.

thetical state for a diblock copolymer, which is ordered at the temperature of interest). The random mixing approximation applies to the entire lattice of the reference phase (i.e., the composition is uniform, $\phi_{Ai}^* = r_A^i/r^i$), whereas the free energy, with respect to the reference state, is given by[5]

$$\frac{A - A^*}{L_{cop}kT} = \sum_i \Theta_i \left\{ \frac{\ln r^i C}{r^i} - \sum_{A,B} \frac{\phi_{Ai}^* \chi_{AB} \phi_{Bi}^*}{2} \right\} - \sum_{z,A'} \frac{\phi_{A'}(z) u_{A'}(z)}{kT} + \sum_{z,A,B} \frac{\phi_A(z) \chi_{AB} \langle \phi_B(z) \rangle}{2} \quad \text{(B1)}$$

It is clearly seen from Figure 12 that the correct long period is predicted when $\chi_{PS/PV2P} = 0.10$. The dotted curve in Figure 12 is for $\chi_{PS/PV2P} = 0.10$ but when the chain stiffness is not included in the calculation. It is concluded that if the chain stiffness is not taken into account, one cannot achieve good agreement between experimental and SCF results for *both* the long period of the lamellar structure and the interfacial width. Once more it is emphasized that this effective χ (which includes the effects of the capillary waves) leads to a self-consistent description of the data;[36] its arithmetic value should not be compared with those estimated by other procedures (e.g., 0.1092 in ref 54 or 0.0724 in ref 55).

References and Notes

(1) Milner, S. T. *Science* **1991**, *251*, 905. Halperin, A.; Tirrell, M.; Lodge, T. P. *Adv. Polym. Sci.* **1992**, *100*, 31.

(2) Szleifer, I.; Carignano, M. A. *Adv. Chem. Phys.* **1986**, *94*, 165. Szleifer, I. *Curr. Opin. Colloid Interface Sci.* **1986**, *1*, 416.

(3) Zhao, B.; Brittain, W. J. *Prog. Polym. Sci.* **2000**, *25*, 677.

(4) Marques, C.; Joanny, J. F.; Leibler, L. *Macromolecules* **1988**, *21*, 1051. Marques, C.; Joanny, J. F. *Macromolecules* **1989**, *22*, 1458.

(5) Evers, O. A.; Scheutjens, J. M. H. M.; Fleer, G. H. *Macromolecules* **1990**, *23*, 5221. Evers, O. A.; Scheutjens, J. M. H. M.; Fleer, G. H. *J. Chem. Soc., Faraday Trans.* **1990**, *86*, 1333.

(6) Whitmore, M. D.; Noolandi, J. *Macromolecules* **1990**, *23*, 3321. Baranowski, R.; Whitmore, *J. Chem. Phys.* **1995**, *103*, 2343.

(7) Hadziioannou, G.; Patel, S.; Granick, S.; Tirrell, M. *J. Am. Chem. Soc.* **1986**, *108*, 2896. Taunton, H. J.; Toprakcioglu, C.; Fetters, L. J.; Klein, J. *Macromolecules* **1988**, *21*, 3333.

(8) Motschmann, H.; Stamm, M.; Toprakcioglu, C. *Macromolecules* **1991**, *24*, 3681. Dorgan, J. R.; Stamm, M.; Toprakcioglu, C.; Jérôme, R.; Fetters, L. J. *Macromolecules* **1993**, *26*, 5321.

(9) Field, J. B.; Toprakcioglu, C.; Ball, R. C.; Stanley, H. B.; Dai, L.; Barford, W.; Penfold, J.; Smith, G.; Hamilton, W. *Macromolecules* **1992**, *25*, 434.

(10) Field, J. B.; Toprakcioglu, C.; Dai, L.; Hadziioannou, G.; Smith, G.; Hamilton, W. *J. Phys. II Fr.* **1992**, *2*, 2221.

(11) Kent, M. S.; Lee, L. T.; Farnoux, B.; Rondelez, F. *Macromolecules* **1992**, *25*, 6240. Kent, M. S.; Lee, L. T.; Factor, B.; Rondelez, F.; Smith, G. S. *J. Chem. Phys.* **1995**, *103*, 2320.

(12) Budkowski, A.; Steiner, U.; Klein, J.; Fetters, L. J. *Europhys. Lett.* **1992**, *20*, 499. Budkowski, A.; Klein, J.; Steiner, U.; Fetters, L. J. *Macromolecules* **1993**, *26*, 2470. Budkowski, A.; Klein, J.; Fetters, L. J. *Macromolecules* **1995**, *28*, 8571. Budkowski, A.; Klein, J.; Fetters, L. J.; Hashimoto, T. *Macromolecules* **1995**, *28*, 8579. Rysz, J.; Bernasik, A.; Ermer, H.; Budkowski, A.; Brenn, R.; Hashimoto, T.; Jedlinski, J. *Europhys. Lett.* **1997**, *40*, 503.

(13) Petitjean, S.; Ghitti, G.; Jérôme, R.; Teyssié, Ph.; Marien, J.; Riga, J.; Verbist, J. *Macromolecules* **1994**, *27*, 4127.

(14) Kunz, K.; Anastasiadis, S. H.; Stamm, M.; Schurrat, T.; Rauch, F. *Eur. Phys. J., B* **1999**, *7*, 411. Anastasiadis, S. H.; Retsos, H.; Kunz, K.; Toprakcioglu, C.; Smith, G.; Hadziioannou, G.; Gill, R.; Stamm, M. *Polym. Prepr.* **1999**, *40* (2), 116.

(15) Wakharkar, V. S.; Russell, T. P.; Deline, V. R. In *Polymer Based Molecular Composites*; Schaefes, D. W., Mark, J. E., Eds.; MRS Symposium Proceedings 171; Materials Research Society: Warrendale, PA, 1990; p 343.

(16) Green, P. F.; Russell, T. P. *Macromolecules* **1992**, *25*, 783.

(17) Esselink, F. J.; Semenov, A. N.; ten Brinke, G.; Hadziioannou, G.; Oostergetel, G. T. *Phys. Rev. B* **1993**, *46*, 13451.

(18) Liu, Y.; Schwarz, S. A.; Zhao, W.; Quinn, J.; Sokolov, J.; Rafailovich, M.; Iyengar, D.; Kramer, E. J.; Dozier, W.; Fetters, l. J.; Dickman, R. *Europhys. Lett.* **1995**, *32*, 211.

(19) Oslanec, R.; Composto, R. J.; Vlcek, P. *Macromolecules* **2000**, *33*, 2200. Oslanec, R.; Vlcek, P.; Hamilton, W. A.; Composto, R. J. *Phys. Rev. E* **1997**, *56*, R2383.

(20) Russell, T. P.; Anastasiadis, S. H.; Menelle, A.; Felcher, G. P.; Satija, S. K. *Macromolecules* **1990**, *24*, 1575. Green, P. F.; Russell, T. P. *Macromolecules* **1991**, *24*, 2931.

(21) Shull, K. R.; Kramer, E. J.; Hadziioannou, G.; Tang, W. *Macromolecules* **1990**, *23*, 4780. Shull, K. R.; Winey, K. I.; Thomas, E. L.; Kramer, E. J. *Macromolecules* **1991**, *24*, 2748. Dai, K. H.; Kramer, E. J.; Shull, K. R. *Macromolecules* **1992**, *25*, 220.

(22) Zhao, X.; Zhao, W.; Rafailovich, M. H.; Sokolov, J.; Russell, T. P.; Kumar, S.; Schwarz, S. A.; Wikiens, B. J. *Europhys. Lett.* **1991**, *15*, 725. Zhao, X.; Zhao, W.; Zheng, X.; Rafailovich, M. H.; Sokolov, J.; Schwarz, S. A.; Pudensi, M. A. A.; Russell, T. P.; Kumar, S. K.; Fetters, L. J. *Phys. Rev. Lett.* **1992**, *69*, 776.

(23) Jones, R. A. L.; Norton, L. J.; Shull, K. R.; Kramer, E. J.; Felcher, G. P.; Karim, A.; Fetters, L. J. *Macromolecules* **1992**, *25*, 2359.

(24) Clarke, C. J.; Jones, R. A. L.; Edwards, J. L.; Shull, K. R.; Penfold, J. *Macromolecules* **1995**, *28*, 2042.

(25) Alexander, S. *J. Phys. (Paris)* **1977**, *38*, 983. de Gennes, P. G. *Macromolecules* **1980**, *13*, 1069. de Gennes, P. G. *Adv. Colloid Interface Sci.* **1987**, *27*, 189.

(26) Leibler, L. *Makromol. Chem., Macromol. Symp.* **1988**, *16*, 1.

(27) Zhulina, E. B.; Borisov, O. V. *J. Colloid Interface Sci.* **1990**, *144*, 507.

(28) Shull, K. R. *J. Chem. Phys.* **1991**, *94*, 5723. Shull, K. R. *Macromolecules* **1996**, *29*, 2659.

(29) Aubouy, M.; Raphaël, E. *J. Phys. II France* **1993**, *3*, 443. Raphaël, E.; Pincus, P.; Fredrickson, G. H. *Macromolecules* **1993**, *26*, 1996. Aubouy, M.; Fredrickson, G. H.; Pincus, P.; Raphaël, E. *Macromolecules* **1995**, *28*, 2979. Gay, C. *Macromolecules* **1997**, *30*, 5939.

(30) Aubouy, M. Private communication. Aubouy, M. *Phys. Rev. E* **1997**, *56*, 3370.

(31) Scheutjens, J. M. H. M.; Fleer, G. J. *J. Phys. Chem.* **1979**, *83*, 1619. Scheutjens, J. M. H. M.; Fleer, G. J. *J. Phys. Chem.* **1980**, *84*, 178. Scheutjens, J. M. H. M.; Fleer, G. J. *Macromolecules* **1985**, *18*, 1882.

(32) Fleer, G. J.; Cohen Stuart, M. A.; Scheutjens, J. M. H. M.; Cosgrove, T.; Vincent, B. *Polymers at Interfaces*; Chapman and Hall: Cambridge, U.K., 1993.

(33) Fischel, L. B.; Theodorou, D. N. *J. Chem. Soc., Faraday Trans.* **1995**, *91*, 2381.

(34) Terzis, A. F.; Theodorou, D. N.; Stroeks, A. *Macromolecules* **2000**, *33*, 1385.

(35) Anastasiadis, S. H.; Chrissopoulou, K.; Fytas, G.; Appel, M.; Fleischer, G.; Adachi, K.; Gallot Y. *Acta Polym.* **1996**, *47*, 250.

(36) Anastasiadis, S. H.; Retsos, H.; Toprakcioglu, C.; Menelle, A.; Hadziioannou G. *Macromolecules* **1998**, *31*, 6600.
(37) Anastasiadis, S. H.; Russell, T. P.; Satija, S. K.; Majkrzak, C. F. *Phys. Rev. Lett.* **1989**, *62*, 1852. Anastasiadis, S. H.; Russell, T. P.; Satija, S. K.; Majkrzak, C. F. *J. Chem. Phys.* **1990**, *92*, 5677.
(38) Russell, T. P. *Mater. Sci. Rep.* **1990**, *5*, 171.
(39) Anastasiadis, S. H.; Hadziioannou, G.; Boerma, D.; Smulders, P., Unpublished data.
(40) Shull, K. R.; Kramer, E. J.; Hadziioannou, G.; Tang, W. *Macromolecules* **1990**, *23*, 4780. Shull, K. R.; Winey, K. I.; Thomas, E. L.; Kramer, E. J. *Macromolecules* **1991**, *24*, 2748. Dai, K. H.; Kramer, E. J.; Shull, K. R. *Macromolecules* **1992**, *25*, 220.
(41) Semenov, A. N. *Macromolecules* **1992**, *25*, 4967.
(42) Edwards, S. F. *Proc. Phys. Soc.* **1965**, *85*, 613. Helfand, E.; Tagami, Y. *J. Polym. Sci. B* **1971**, *9*, 741.
(43) Theodorou, D. N. *Macromolecules* **1988**, *21*, 1400.
(44) Wijmans, C. M.; Leermakers, F. A. M.; Fleer, G. J. *J. Chem. Phys.* **1994**, *101*, 8214.
(45) A Kuhn segment, l_K, is defined such that a chain will have the same mean-square end-to-end distance and maximally extended length in the Kuhn representation as measured experimentally, i.e., $\langle R^2 \rangle = C_\infty n_b l_b^2 = r_K l_K^2$ and $r_K l_K = n_b l_b \sin(\theta_b/2)$. Therefore, $l_K = C_\infty l_b [\sin(\theta_b/2)]^{-1}$. r_K is the number of Kuhn segments.
(46) Mattice, W. L.; Suter, V. W. *Conformational Theory of Large Molecules*; John Wiley & Sons: New York, 1994.
(47) Tonelli, A. E. *Macromolecules* **1985**, *18*, 2579.
(48) van Krevelen, P. W. *Properties of Polymers*; Elsevier: New York, 1997.
(49) Mark, J. E. *Physical Properties of Polymers Handbook*; American Institute of Physics: New York, 1996.
(50) Semenov, A. N. *Zh. Eksp. Teor. Fiz.* **1985**, *88*, 1242 [*Sov. Phys. JETP* **1985**, *61*, 733].
(51) Milner, S. T.; Witten, T. A.; Cates, M. E. *Macromolecules* **1988**, *21*, 2610. Zhulina, E. B.; Borisov, O. V.; Pryamitsyn, V. A. *Polym. Phys. USSR* **1989**, *31*, 205.
(52) Powell, M. J. D. In *Numerical Methods for Nonlinear Algebraic Equations*; Rabinowitz, P., Ed.; Gordon and Breach: New York, 1970.
(53) Russell, T. P.; Hjelm, R. P.; Seeger, P. A. *Macromolecules* **1990**, *23*, 890. Russell, T. P. *Macromolecules* **1993**, *26*, 5819.
(54) Dai, K. H.; Kramer, E. J. *Polymer* **1994**, *35*, 157.
(55) Matsushita, Y.; Mori, K.; Sagushi, R.; Nakao, Y.; Noda, I.; Nagasawa, M. *Macromolecules* **1990**, *23*, 4313. Torikai, N.; Noda, I.; Karim, A.; Satija, S. K.; Han, C. C.; Matsushita, Y.; Kawakatsu, T. *Macromolecules* **1997**, *30*, 2907.

MA011174J